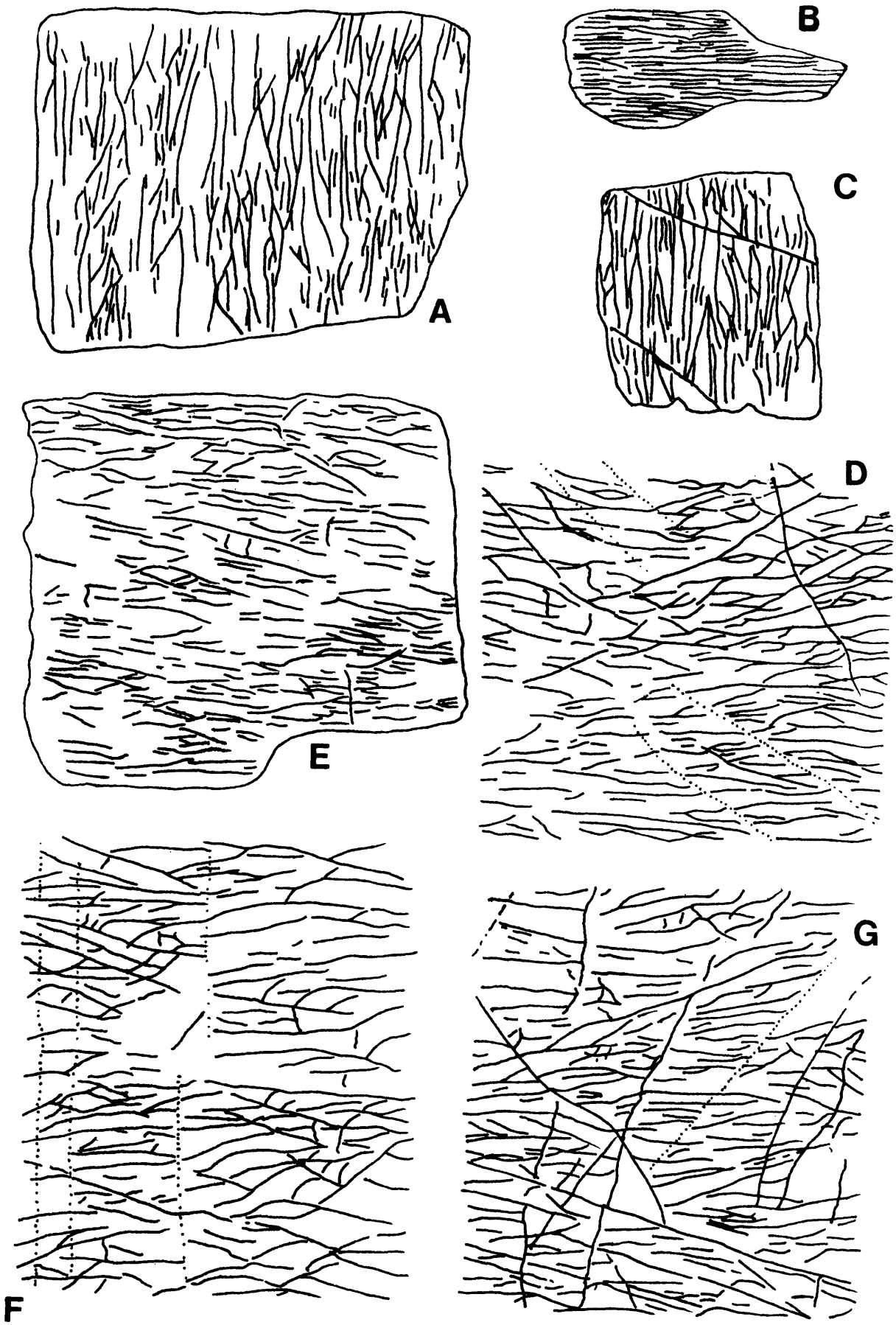


Fig. 21: Patterns of typical cleavage traces analysed by the chart digitizer. A - Specimen 1, B - Specimen B, C - Specimen 7, D - Specimen 8, E - Specimen 2-12, F - Specimen 2-13, G - Specimen 2-14. All magnifications x 1.

electronic chart digitizer at the Division of Mineral Physics, CSIRO, North Ryde, and results calculated by program GOLLUM (see Appendix II). Initially two specimens were digitised (Specimen A, Plate 5A, and Specimen B, Fig.21B) and results for lengths and spacings are shown in Figure 22. On graphs of length versus orientation from the dominant cleavage plane (Figs. 23A and B) the pattern as predicted by the model in Chapter 1 (p.25-29) was not observed. Instead, a distribution to both sides of the dominant cleavage plane occurred.

The real distributions exhibit a close similarity to the theoretical curves, indicating that the cleavage planes are diverging on both sides away from the dominant cleavage plane. Because of the unusual pattern encountered it was decided to examine more specimens, particularly of "fracture" cleavage to see if similar patterns could be recognised. Specimen B for slaty cleavage has an almost parallel orientation with only two cleavage planes out of a total of 66 diverging more than 8° from the dominant cleavage plane.

Subsequently the lengths and orientations of cleavage planes in fourteen specimens and photographs were determined using the electronic digitizer. Specimens were collected from four main localities within the Block and can be grouped into five divisions with respect to the orientation of the bedding and mesoscopic folds:

(a) the plane of the specimen is parallel to the ac-plane, and bedding and the dominent cleavage are subvertical (e.g. Specimen 1, Figs. 21A and 24A);

(b) similar to (a) except that the bedding is subhorizontal (e.g. Specimen 2-13, Figs. 21F and 26C);

(c) similar to (a) except that the bedding has an approximate east-west strike and dips moderately to the north (e.g. Specimen 2, Plate 6B and Fig. 25A);

(d) similar to (c) except the bedding dips moderately to the south (e.g. Specimen 2-12, Figs. 2-12 and 26C); and

(e) the plane of the specimen is subhorizontal and hence not in the ac-plane (e.g. Specimen 3A, Plate 6A and Fig. 26A).

A summary of results is presented in Table 3 and Figs. 23-26. For most specimens there is a symmetrical distribution of points on both sides of the dominant cleavage plane, and this cannot be explained by the

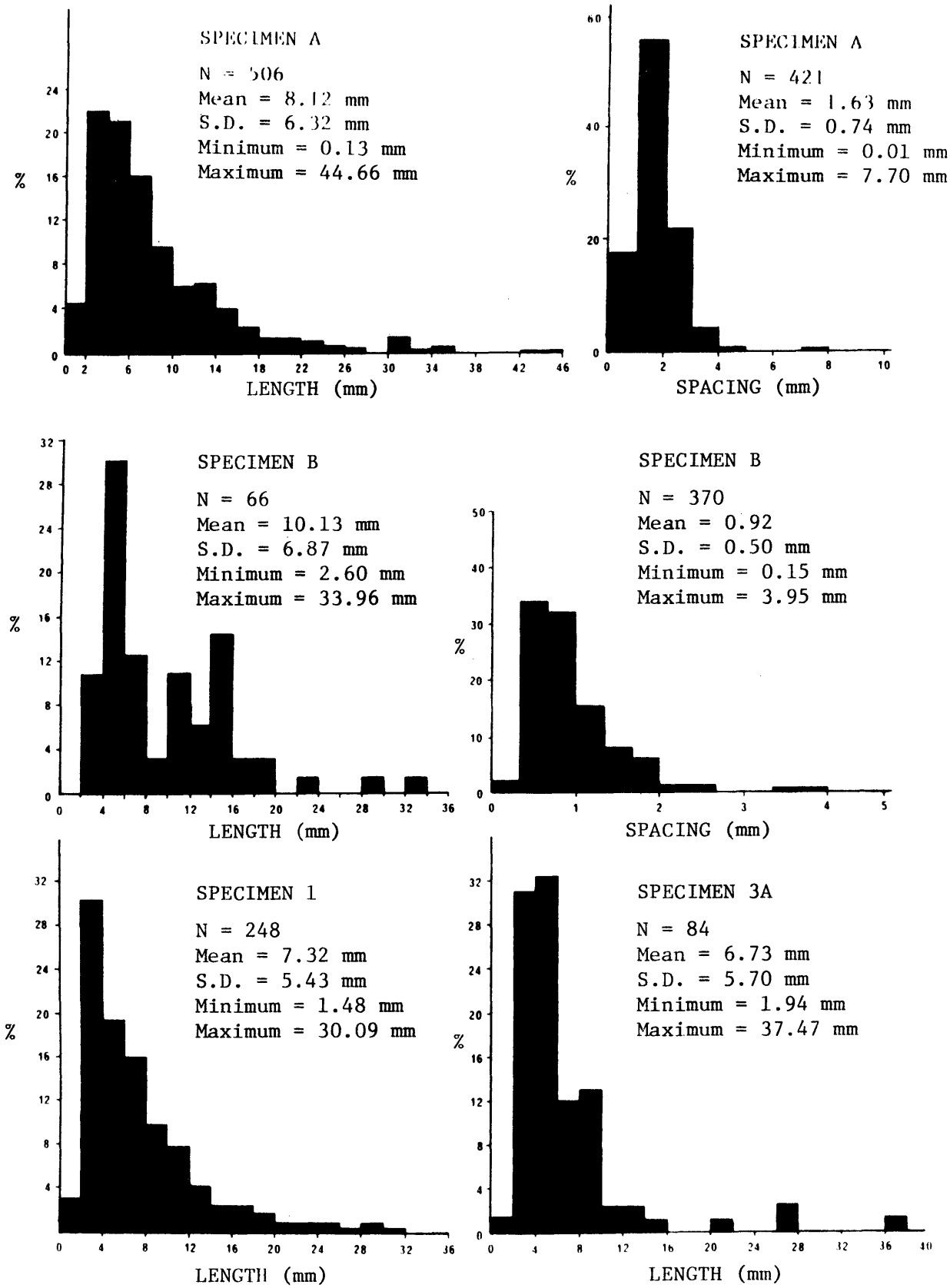


Fig. 22: Results for lengths and spacings of cleavage planes in specimens analysed by an electronic chart digitizer.

Table 3: Summary of results for cleavage patterns from the Coffs Harbour Block, and comparison with theoretical curves

| Sample Number | Location | Orientation of bedding | Orientation of dominant cleavage | Orientation of sample | Pattern of sample on 1 v. θ graph and comparison with theoretical model for $1 = \frac{s}{\sin \theta}$ |
|---|---|---|---|---|---|
| A | Unit D, Coramba Beds Woolgoolga GR 6330 2695 | unknown | unknown | unknown | symmetrical distribution about dominant cleavage plane, for S = 1.63 mm 53.6% of data occur beneath the theoretical curve |
| B | Brooklana Beds, GR 5768 2792 | not observed | 134/N/89 | perpendicular to cleavage | small variation in orientation about the dominant cleavage plane. For S = 0.92 mm 89.4% of data are beneath the curve |
| 1 | Unit D, Coramba Beds Arrawarra GR 6324 2756 | 072/N/86 | 076/S/82 | 166/E/82, in ac-plane on limb of monocline | symmetrical distribution. For S = 2 mm 83.9% of data occur beneath the theoretical curve |
| 6 | Unit A, Coramba Beds Mutton Bird Island GR 6262 2458 | 074/S/70 | 100/S/83 | strike approximately N-S, subvertical dip | symmetrical distribution. Using S = 3 mm 84.2% of data fall under the theoretical curve |
| 7 | Same location as Specimen 6 | 074/S/70 | 100/S/83 | strike approximately N-S, dip about 30°W, in ac-plane | symmetrical distribution. 88.3% of points fall beneath the curve for S = 2 mm |
| 8 | Brooklana Beds, Coffs Harbour GR 6262 2450 | 134/N/80 | 127/N/86 | normal to cleavage in the vertical plane | symmetrical distribution with 86.6% of data occurring under the theoretical curve for S = 2 mm |
| 2 | same as Specimen 1 | 087/N/32 | 075/N/78 | 000/E/70 in ac-plane | symmetrical distribution. For S = 2 mm 79.0% of data are under the curve |
| 3B | same as Specimen 1 | similar to Specimen 2 | | ac-plane (subvertical) | one-sided distribution similar to the theoretical model, 75.4% of data occur beneath the theoretical curve of S = 3 mm |

Table 3: (continued)

| Sample Number | Location | Orientation of bedding | Orientation of dominant cleavage | Orientation of sample | Pattern of sample on 1 v. θ graph and comparison with theoretical model for $1 = \frac{s}{\sin \theta}$ |
|---|---|---|---|---|---|
| 1-30A, 1-30B | same as Specimen 1 | 062/N/40 | $S_{1a}$ 081/N/82<br>$S_{1b}$ 087/S/85 | in ac-plane | A - symmetrical, S = 3 mm, 86.3% of data fall beneath curve<br>B - one sided distribution but reverse pattern to the predicted one, for S = 3.5 mm, 70.5% of points are under the curve |
| 4 | same as Specimen A | 027/W/38 (hinge of fold) | 102/S/80 | 010/E/62, in ac-plane | symmetrical distribution. For S = 2 mm 74.3% is under the curve |
| 5 | same as Specimen A | unknown | 100/S/80 | horizontal | symmetrical with 81.0% of data beneath curve of S = 2 mm |
| 3A | same as Specimen 3B | same as specimen 3B | | horizontal | curve fits model. For S = 4.5 mm 91.7% of data fall beneath curve |
| 2-12, 2-13, 2-14 | same location as specimen A. Collected from limbs and hinge of an anticline | 12 E-W strike dip to south<br>13-horizontal<br>14-dip to north | strike is E-W with subvertical dip | all specimens in ac-plane | all show a symmetrical distribution, with a greater scatter in 12 and 14 than in 13 from the hinge area. For 12 S = 3 mm and 85.3% is beneath curve. Using 5 mm for 13 gives 88.2% beneath curve. For 14 with S = 3 mm, 79.7% of data fall under the curve |

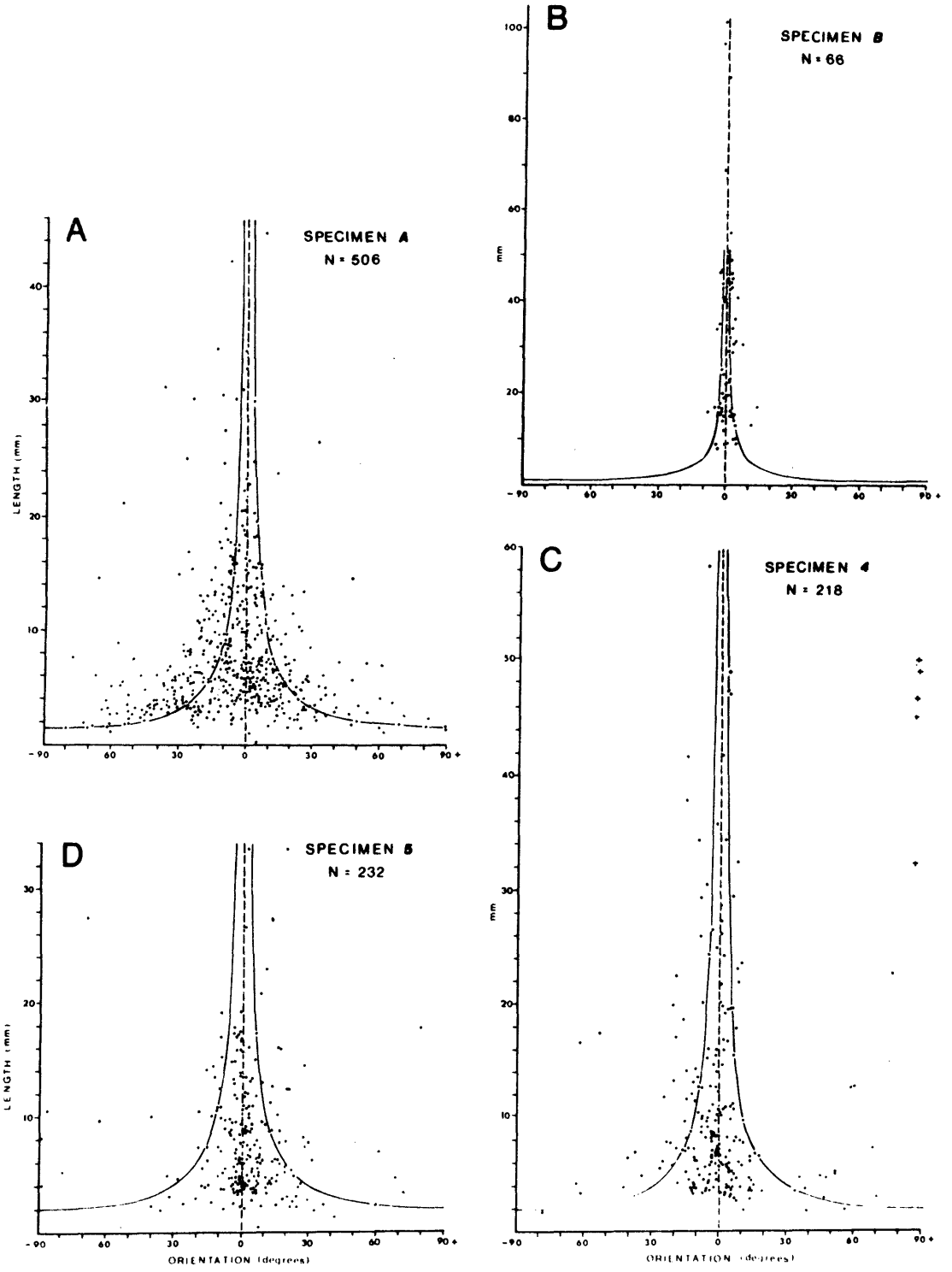


Fig. 23: Graphs of length of cleavage plane versus orientation from the dominant cleavage plane for specimens from the Coffs Harbour Sequence.

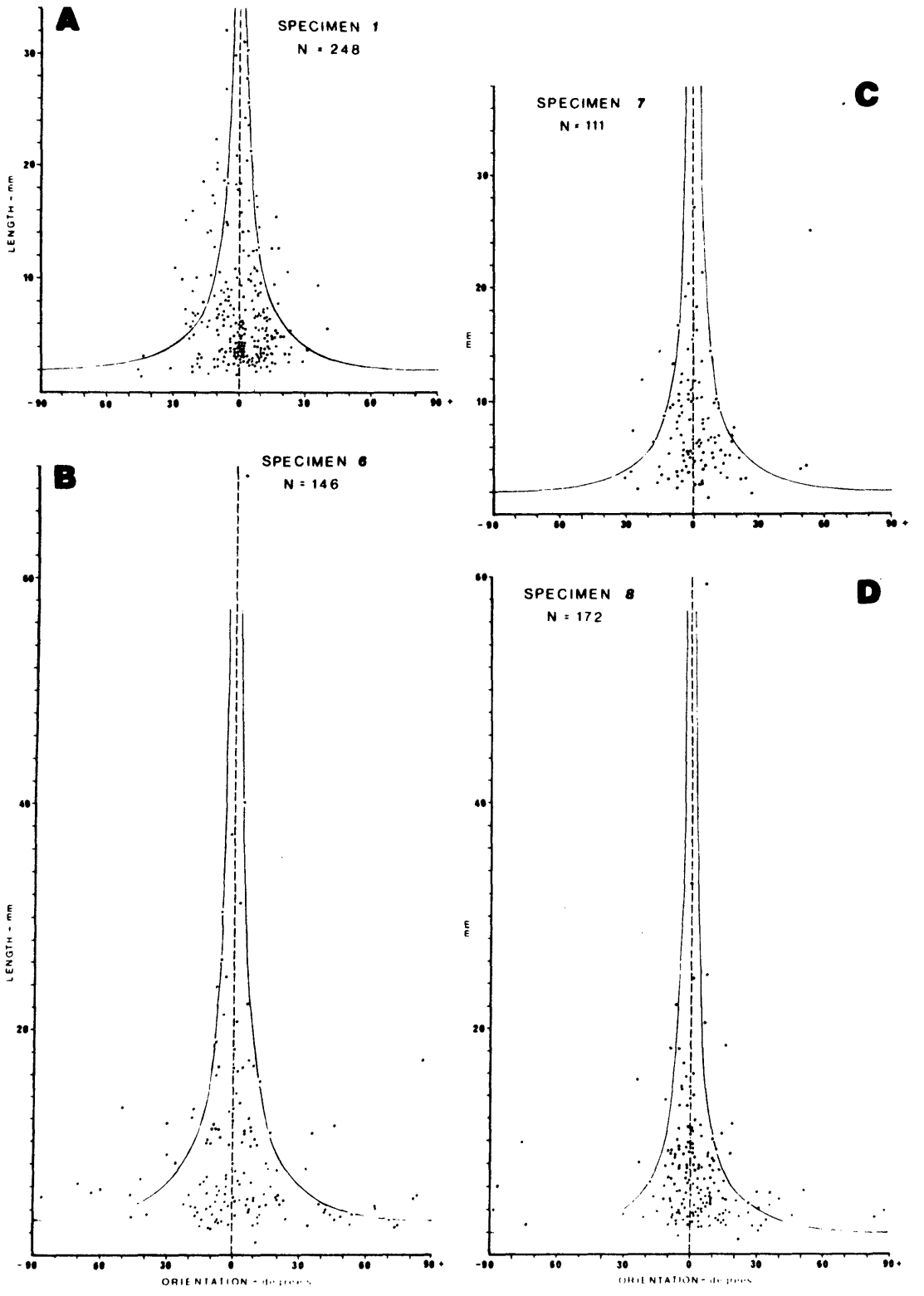


Fig. 24: Graphs of length of cleavage plane versus orientation from the dominant cleavage plane for specimens from the Coffs Harbour Sequence.

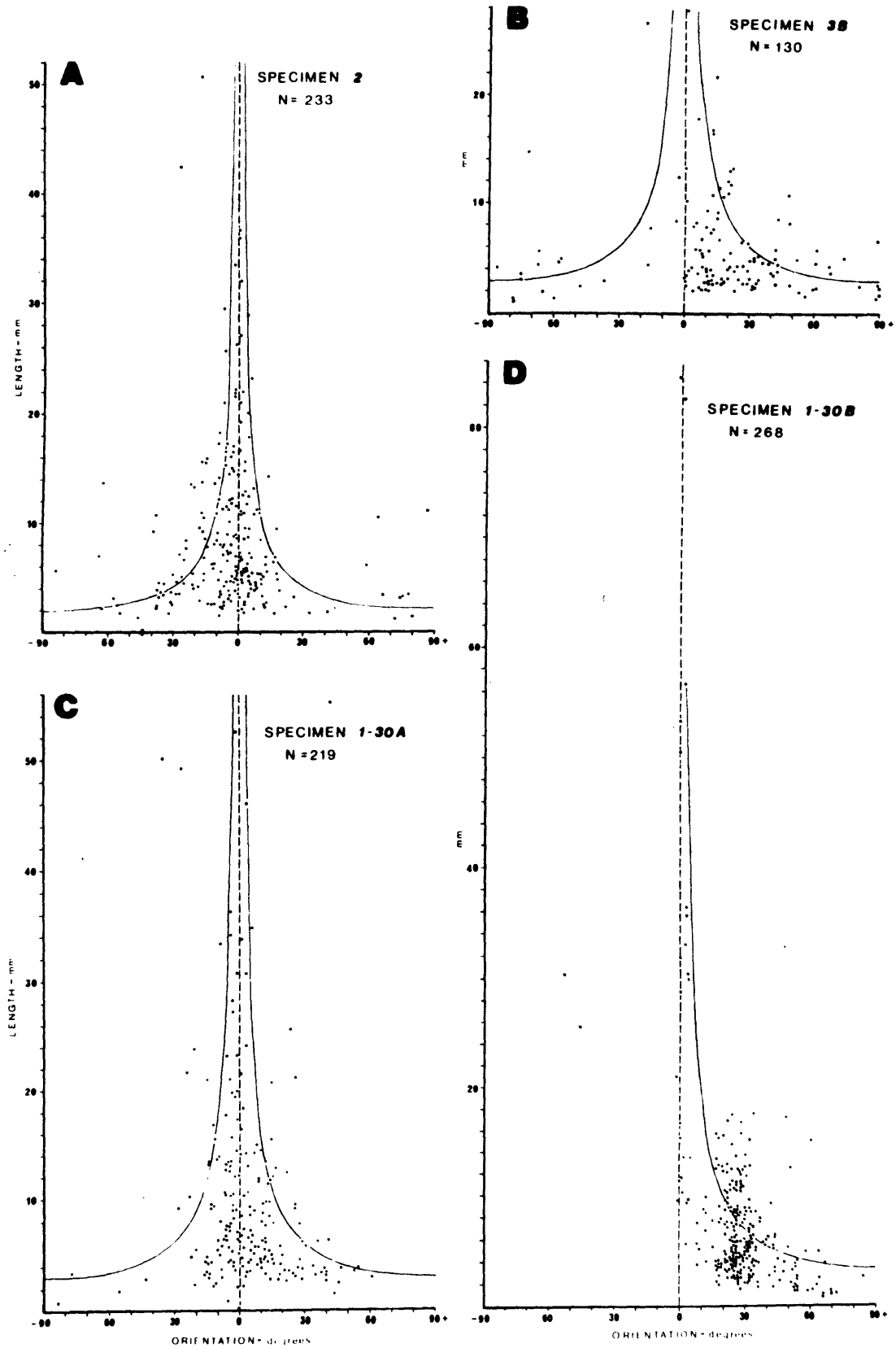


Fig. 25: Graphs of length of cleavage plane versus orientation from the dominant cleavage plane for specimens from the Coffs Harbour Sequence.

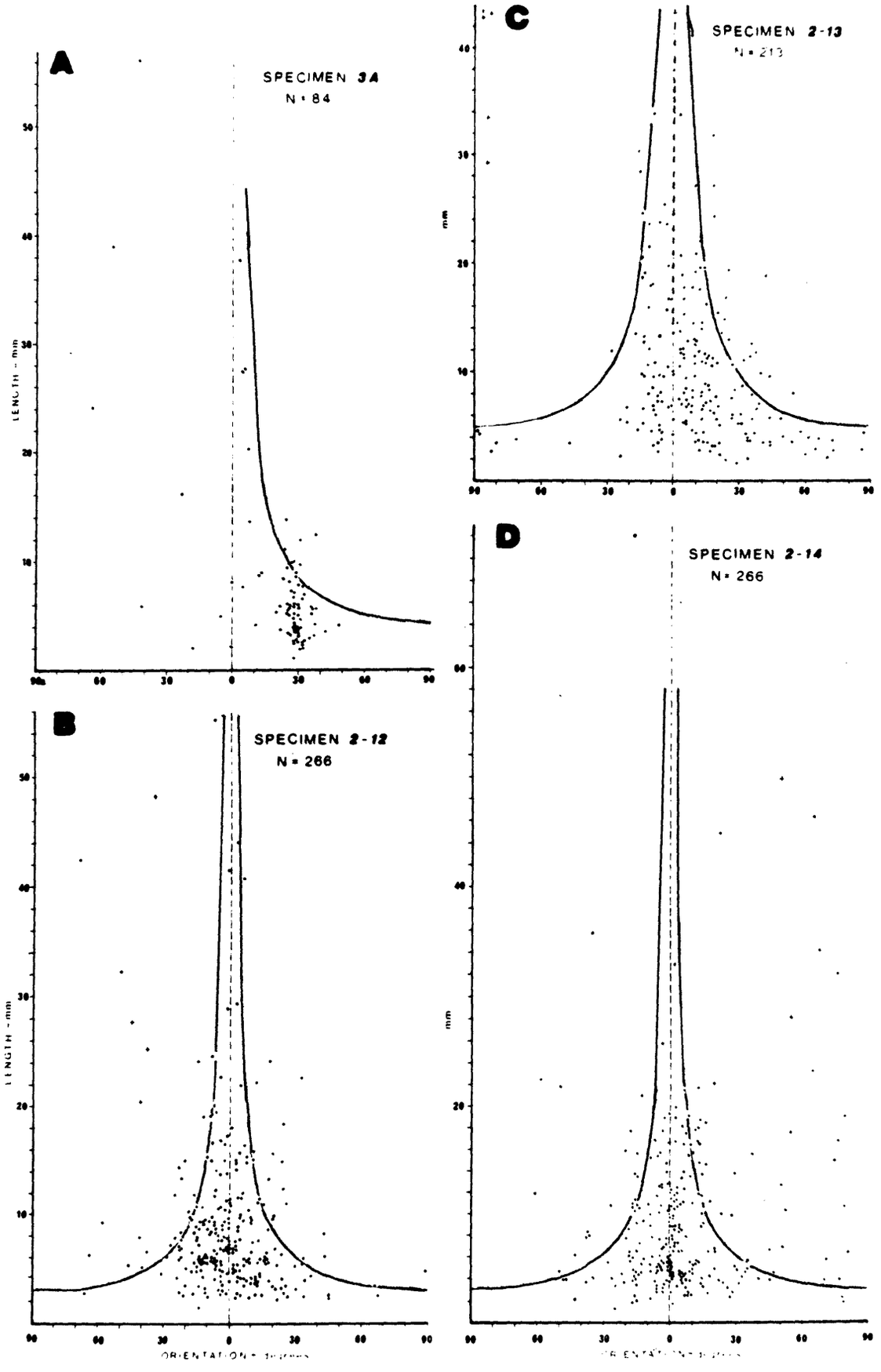


Fig. 26: Graphs of length of cleavage plane versus orientation from the dominant cleavage plane for specimens from the Coffs Harbour Sequence.

theoretical model. In three cases (Specimen 3A, Fig. 26A; Specimen 3B, Fig. 25B; Specimen 1-30B, Fig. 25D) the data fit the theoretical model. However in one of these cases (Specimen 1-30B) the pattern observed is the reverse of that expected in relation to the orientation of the bedding and the fold. Hence, while two cases agree with the model in exhibiting diminishing lengths of cleavage traces in one direction away from the dominant cleavage plane, most cases fit the equation of the model but show a symmetrical distribution rather than a heavily skewed one. What is the significance of this pattern? The pattern suggests that on the limbs of folds the cleavage planes consist of a series of traces which diverge on both sides away from the most dominant (or longest) set of cleavage planes.

(b) Mechanisms of cleavage development

Many writers follow the work of Harker (1885), Van Hise (1896) and Leith (1905) in accepting that deformed objects such as fossils, tuff lapilli and ooids show that slaty cleavage develops normal to the direction of maximum finite shortening. This geometrical relationship has been accepted by many workers and supported by Cloos (1947), de Sitter (1954), Gonzalez-Bonorino (1960) and many others. Siddans (1972) presents a review of slaty cleavage and accepts the above point of view which is also supported by the theoretical models of Dieterich (1969).

An opposing view that slaty cleavage forms parallel to planes of maximum shearing stress was introduced by Becker (1893) and is followed by Turner (1948), Fairbain (1949) and Voll (1960), but is not favoured by many later workers because it is in conflict with the results of strain analyses (see techniques of Ramsay 1967, Chapter 5).

While a majority of structural geologists support the geometrical relationships outlined by Siddans (*op. cit.*) there is still considerable debate as to the mechanisms by which slaty cleavage developed. The contentious issue is the origin of the planar fabric defined by the parallel arrangement of minerals such as mica and chlorite which have the (001) plane parallel to the slaty cleavage. The two main processes debated are the mechanical rotation of existing particles against the crystallisation of new minerals.

Turner (1948) and Turner and Weiss (1963, p.440) have reviewed the mechanisms thought to be responsible for preferred orientations of mica. Of the six mechanisms considered by Turner and Weiss the following appear to be applicable to the slaty cleavage developed in the southern part of the Coffs Harbour Block:

1. bodily rotation of small mica flakes into the plane normal to the axis of maximum compressive stress during transformation of mudstone to slate;
2. syntectonic growth of mica crystals with their longest dimensions normal to the axis of maximum compressive stress;
3. syntectonic and post-tectonic crystallisation of mica in orientations controlled by existing visible s-surfaces and lineations. The most common orientation is that where the crystals grow with their longest dimensions (001) parallel to the controlling s-surface or lineation, and is known as mimetic crystallisation.

It is possible that any one or all three mechanisms contributed to the development of the slaty cleavage. These mechanisms rely on the hypothesis that the cleavage developed after the rocks were compacted and lithified. In recent years an hypothesis proposed by Maxwell (1962) has provided an alternative whereby slaty cleavage can develop in unlithified sediments. Maxwell proposed that slaty cleavage is produced by tectonic dewatering of muddy sediments under a high pore-water pressure prior to lithification.

The main evidence found by Maxwell to support his hypothesis was the injection of sandstone dykes parallel to the cleavage, and hence the sandstone must have been highly mobile at the time of injection. Maxwell claimed the rapid application of tectonic stress induced high pore-water pressures, drastically reducing internal friction. This led to rotation of mineral grains and accompanying mass transportation parallel to the axial planes of folds which were developing, and the production of the preferred mineral orientation which is characteristic of slaty cleavage.

Wood (1974) in a comprehensive review rejects Maxwell's (1962) hypothesis of tectonic dewatering as a universal explanation for slaty cleavage and concludes that the recrystallisation hypothesis of Van Hise (1896) is more acceptable. This hypothesis invokes the notion that chemical processes are of greater importance than mechanical processes in producing cleavage. Wood (*op. cit.*) considers that pressure solution transfer as described by Durney (1972) provides an acceptable mechanism for the development of slaty cleavage.

(c) Significance of cleavage from the Coffs Harbour Block

An analogous pattern to those described from the Coffs Harbour Block is the development of crenulation cleavage described by Hoeppener (1956) from

the Rheinische Schiefergebirge. Hoeppener envisaged the process as a continuous one, whereby the first (slaty) cleavage ($S_1$) was formed, and then rotated about the b-axis, before the development of a new set of s-surfaces ($S_2$) due to continued compression. After this stage the $S_1$ cleavage in the microlithons between adjacent $S_2$ surfaces become further deformed by flattening.

The pattern observed in the Coffs Harbour Block might be similar to that described by Hoeppener (1956) and the stage reached might be similar to that illustrated by him in his Figures 24a, 24b, 28c, 28d. This raises a problem in that the cleavage described from the Coffs Harbour Block grades with increasing metamorphism and deformation into a true slaty cleavage. In other words the cleavage is produced at a lower grade than the true slaty cleavage and appears to be associated with no noticeable recrystallisation.

Most of the cleavage specimens analysed by the writer are from coastal headlands at Arrawarra and Woolgoolga which are in metamorphic Zone I (prehnite-pumpellyite facies, see Appendix I, Chapter 3 and Map 2). Within this zone there is a conglomerate horizon (GR 5627 3014). The three axes of fifty pebbles in the conglomerate were measured and plotted on the X/Y versus Y/Z graph of Flinn (1956) in which $X > Y > Z$ (Fig. 27A). Also plotted are the deformed and undeformed pebble fields of Flinn (*op. cit.*). The pebbles from the conglomerate in Zone I have a shape similar to those of the undeformed pebbles described by Flinn and consequently have been little affected by deformation. The fine-grained shaly horizons do tend to exhibit more intense deformation textures than coarser-grained units in close proximity but there has been only moderate deformation in Zone I. Support for this conclusion is given by the large interlimb angles of the mesoscopic folds which at Arrawarra have an average value of 103°, and at Woolgoolga of 83° (Fig. 36).

It is concluded that the fracture cleavage patterns discussed here were produced by a deformation of lesser intensity than that which produces slaty cleavage, and it is likely that with further deformation this fracture cleavage grades into slaty cleavage. Both cleavages have an axial-surface orientation (statistically), and show a gradual transition from one to the other.

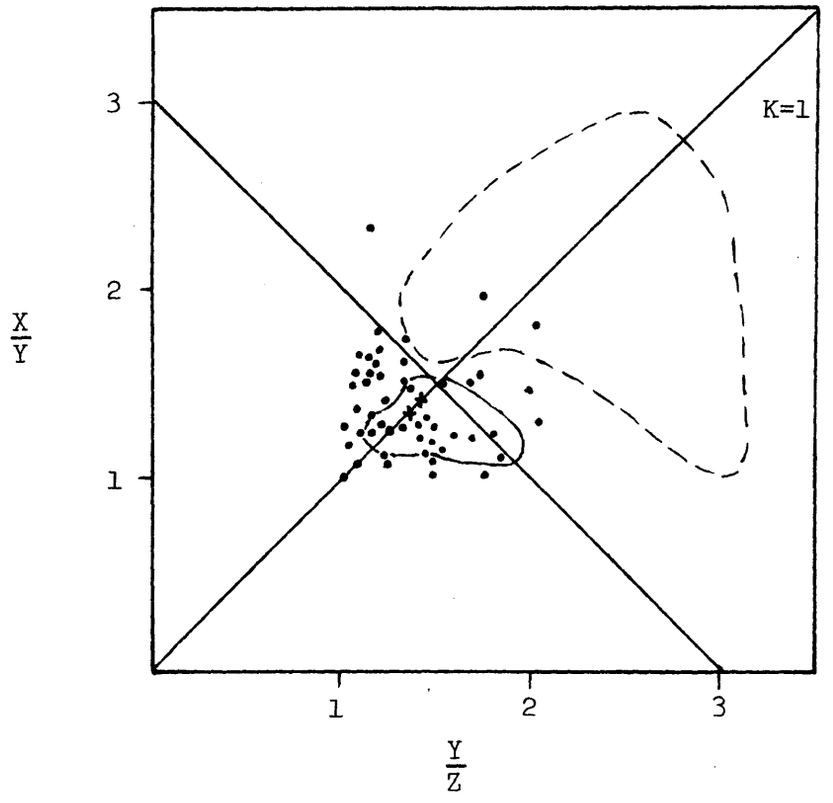


A

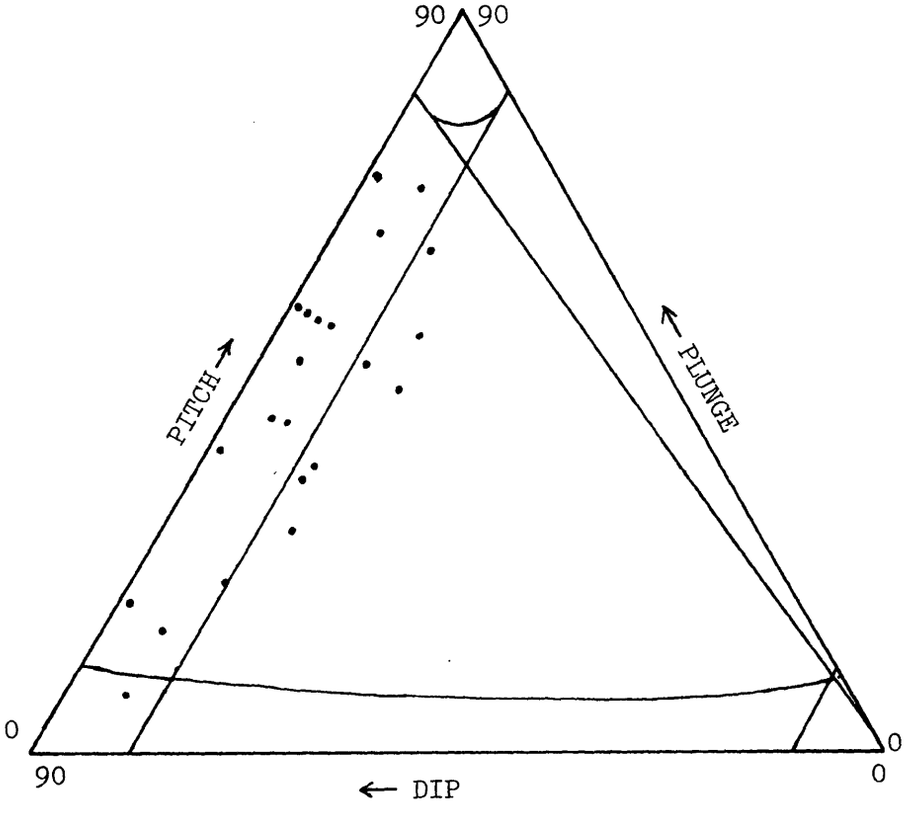


B

Fig. 27 A: Graph of $\frac{X}{Y}$ to $\frac{Y}{Z}$ ratios for clasts from conglomerate in Coramba Beds. • = clast, + undeformed pebble of Flinn (1956), — undeformed pebble field of Flinn, --- deformed conglomerate pebble field of Flinn.

B: Average dip of AS versus average plunge of FA for mesoscopic D1 folds from the coastal headlands (after Rickard, 1971).

2. Linear structures ($L_1$)

The D1 lineation is an L(So x $S_1$) type which more specifically is LIN COM (13, 31) or (13, 32) depending on the lithology in which the lineation is observed. It appears as a faint banding produced by the traces of very thin beds or laminations on the cleavage surfaces, or as parallel cracks on the bedding planes. It is not common because the rocks usually are not well laminated.

3. Mesoscopic folds

D1 mesoscopic folds are abundant throughout the Coffs Harbour Block, but the best exposures are in the coastal headlands from Broomes Head to Bonville Headland. These folds in So change in shape and attitude from north to south in a systematic manner which will be described later.

Symmetrical folds (Plate 7A-D) with limbs of equal lengths are common although asymmetrical folds and disharmonic folds occur (Fig. 28). The fold hinges can be sharp lines, or zones in which the folded surfaces have a constant curvature. The axial surfaces are mainly planar and are often defined by a well developed cleavage. The fold axes observed in the field were in most cases rectilinear. The mesoscopic folds are usually cylindrical or cylindroidal over the scale of the outcrop. Profile shapes commonly change upwards and downwards in a stack of form surfaces, in company with thinning of the limbs of form layers and thickening in the hinges. Wavelengths and amplitudes range from $\lambda$ = 0.3 m, A = 0.15 m to $\lambda$ = 30 m, A = 5 m for D1 folds from the Coffs Harbour Sequence.

Three folds (Fig. 29) with interlimb angles ranging from gentle (146°) to tight (20°) have been selected as representative examples of symmetrical mesoscopic D1 folds from the Coffs Harbour Sequence, and several form surfaces have been used to determine the dimensions in Table 4. Interlimb angles are extremely variable but change systematically through the Block. Within a fold the form surfaces exhibit approximately the same A and $\lambda$ and consequently $\lambda$/L and A/L. The dispersion of the $\lambda$/L and A/L values when plotted against $\theta$ (Fig. 30) is such that the D1 mesoscopic folds occupy an extremely large field on the graphs, in contrast with the very small field for the tight folds in the Redbank River Beds.

Values for the chord ratio (C) indicate the folds are rounded paraboloidal folds. The A/$\lambda$ ratio (Table 4) changes progressively from form surface 1 to surface 7. Hence from fold A through fold B to fold C,

PLATE 7

D1 Mesoscopic Structures from the Coffs Harbour Block

A. Mesoscopic fold in competent sandstone layer from Unit D, Coramba Beds. Woolgoolga Headland (GR 5322 2696). Photograph covers a width of approximately 4m.

B. Symmetrical fold in competent sandstone layer from Unit A, Coramba Beds. Korora Bay (GR 6267 2540). Pencil for scale is 0.14m long.

C. Isoclinal fold closure in siltstone layer, surrounded by more incompetent mudstone. Unit A, Coramba Beds. Charlesworth Headland (GR 6260 2500). Pencil for scale is 0.09m long.

D. Isoclinal folds in siliceous mudstone from Unit A, Coramba Beds. Signal Hill (GR 6310 2615). Brunton compass indicates scale.

E. Movement along cleavage planes to produce folds by the slip mechanism. Unit A, Coramba Beds. Mutton Bird Island (GR 6262 2458). Hammer head in upper left hand corner indicates scale.

F. Refraction of cleavage between a mudstone (lower) layer and a sandstone (upper) layer. Angle through which the cleavage has been refracted is approximately 25°. Unit A, Coramba Beds. Moonee Beach (GR 6276 2570). Pencil for scale is 0.14m long.

A

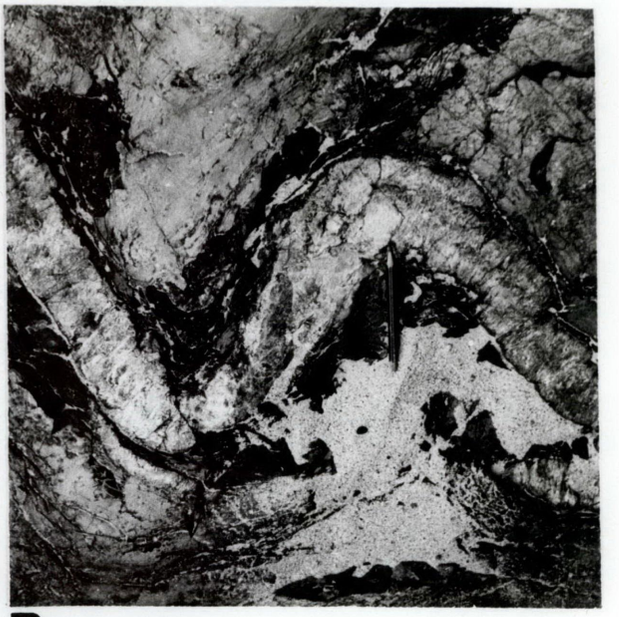

B

C

D

E

F

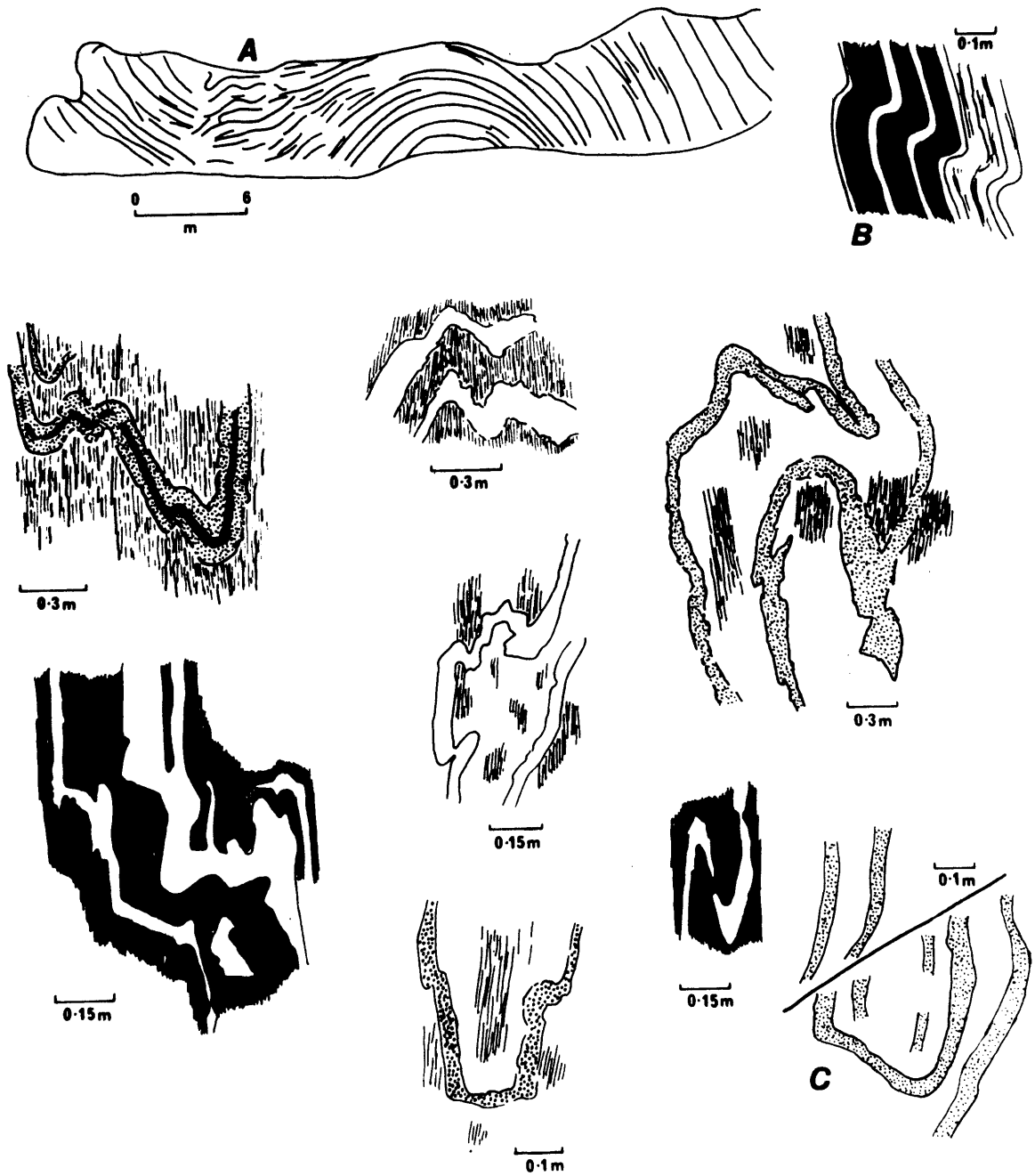


Fig. 28: Profile sketches of asymmetrical and disharmonic folds from the Coffs Harbour Sequence. Fold A - Broomes Head, Fold B - McCauleys Head, Fold C - Sandon Bluffs, Remainder from Charlesworth Head.

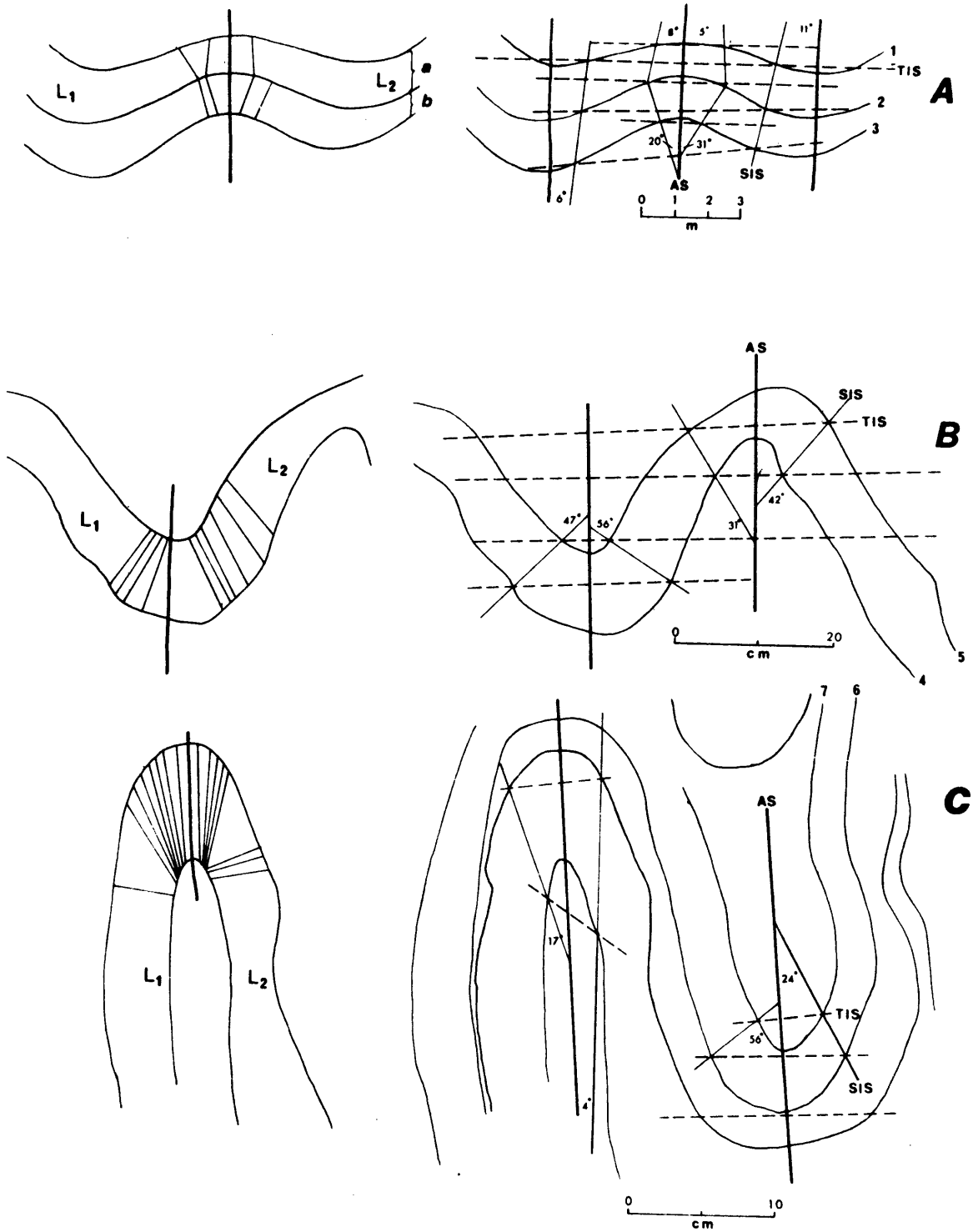


Fig. 29: Dip isogon and inflection surface patterns for mesoscopic D1 folds from the Coffs Harbour Sequence.

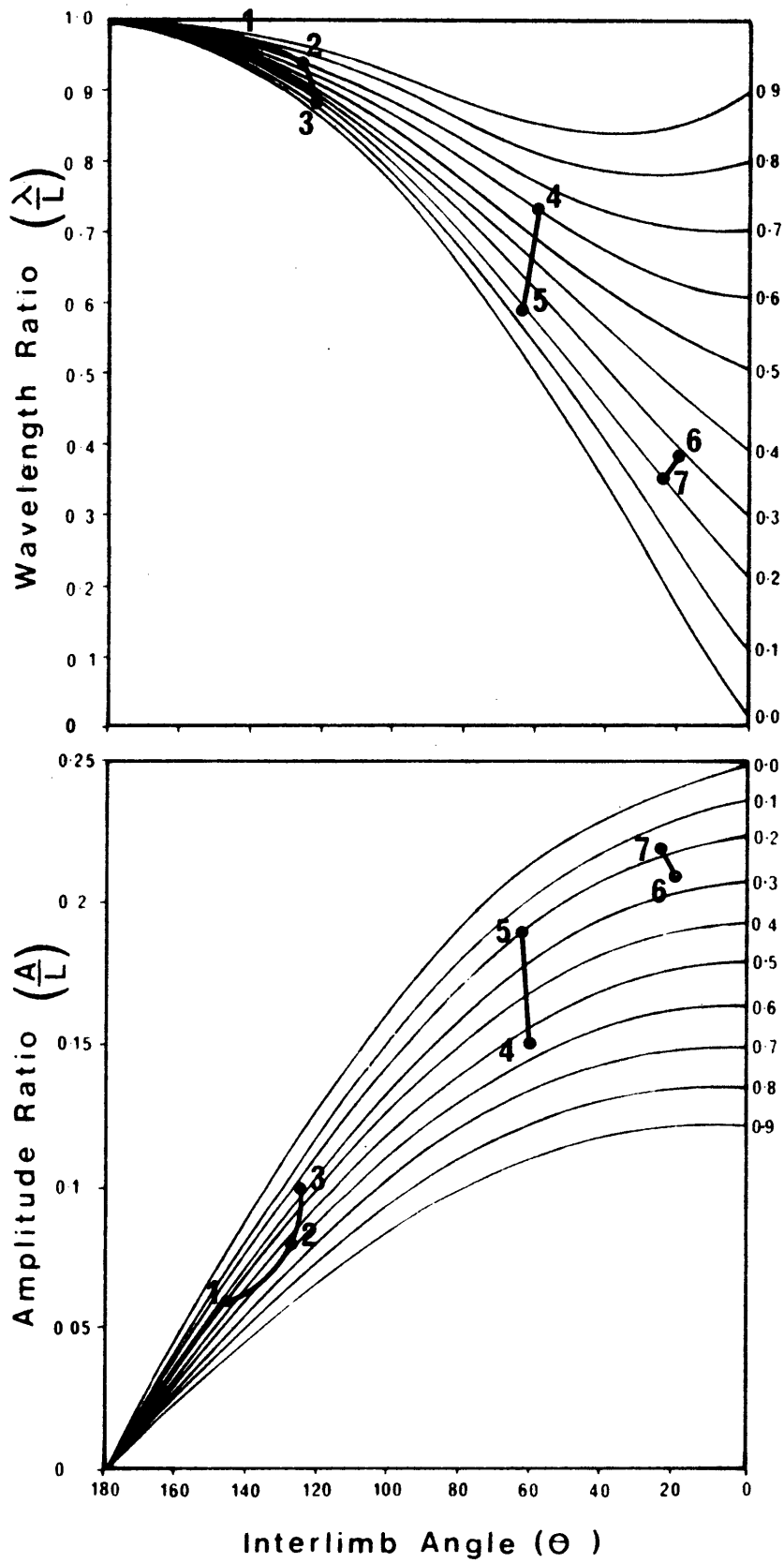


Fig. 30: $\frac{\lambda}{L}$ and $\frac{A}{L}$ versus $\theta$ graphs showing migration paths of folded surfaces of D1 mesoscopic folds from the Coffs Harbour Sequence.

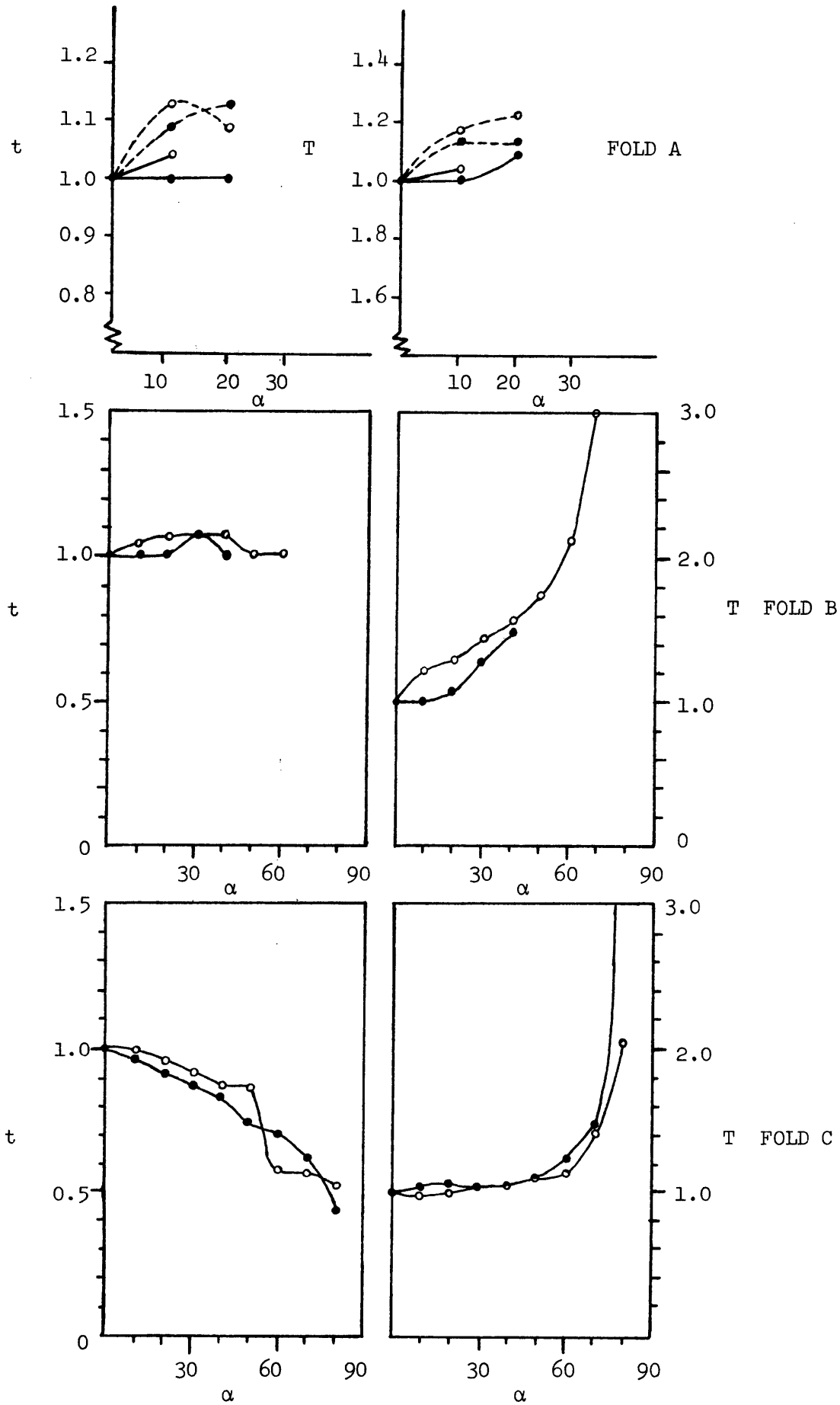


Fig. 31: T and t compared with α for D1 folds from the Coffs Harbour Block. • = Limb 1, o = Limb 2, — Layer a, --- Layer b. Note change in scale for Fold A.

Table 4: Dimensional data for D1 mesoscopic folds from the Coffs Harbour Sequence
Values of c, f, λ, A, Z are given in metres, θ in degrees and V in percent.

| Fold | Folded Surface | θ | c | f | λ | A | V | c/f | λ/L | A/L | A/λ | $Z^a$ | $Z^b$ | Z/L |
|---|---|---|---|---|---|---|---|---|---|---|---|---|---|---|
| Fold A | 1 | 146 | 2.2 | 4.6 | 8.93 | 0.51 | 3 | 0.48 | 0.97 | 0.06 | 0.06 | 0.35 | 0.50 | 0.04 |
| Sandon Bluffs (GR 6468 3214) | 2 | 127 | 2.5 | 4.3 | 8.06 | 0.68 | 6 | 0.58 | 0.94 | 0.08 | 0.08 | 0.38 | 0.90 | 0.04 |
| | 3 | 125 | 1.3 | 4.2 | 7.08 | 0.82 | 14 | 0.31 | 0.86 | 0.10 | 0.12 | 0.58 | 1.00 | 0.07 |
| Fold B | 4 | 60 | 0.20 | 0.34 | 0.50 | 0.10 | 27 | 0.59 | 0.73 | 0.15 | 0.20 | 0.04 | 0.13 | 0.06 |
| Korora Bay (GR 6154 2511) | 5 | 62 | 0.06 | 0.30 | 0.36 | 0.12 | 41 | 0.20 | 0.59 | 0.19 | 0.32 | 0.10 | 0.11 | 0.17 |
| Fold C | 6 | 20 | 0.20 | 0.70 | 0.55 | 0.29 | 61 | 0.29 | 0.39 | 0.21 | 0.53 | 0.21 | 0.20 | 0.15 |
| Signal Hill (GR 6308 2616) | 7 | 25 | 0.14 | 0.70 | 0.49 | 0.30 | 65 | 0.20 | 0.35 | 0.22 | 0.61 | 0.24 | 0.23 | 0.17 |

a Value of Z calculated from formula

b Value of Z measured from folds

the surfaces become progressively more flattened. This is also reflected in the percent shortening (V).

Dip isogons and graphs of T and t versus $\alpha$ for three representative folds (Figs. 29 and 31) show that layer b of fold A and limb 2 of layer a of fold A are in Class 1A of Ramsay (1967) whereas limb 1 of layer a approximates to class 1B. Korsch (1968) treated folds B and C (Fig. 29) using the orthogonal thickness method of Ramsay (1962) and considered that these folds have a relatively constant orthogonal thickness and hence have an approximately parallel geometry. These folds have been re-examined. Fold B equates with class 1A extremely close to class 1B. Fold C approximates more closely to class 1C having weakly convergent dip isogons. This fold has been flattened by 25-33% (from graph of Ramsay 1962, p.315). Because of the similarity in morphology between these folds and other D1 symmetrical folds it is considered that most D1 folds have a class 1A to class 1C geometry. They have developed in competent layers, separated by incompetent layers in which the geometry is of a different class. The folds in the competent layers are considered to have been produced by an initial period of buckling, and in the region of more intense deformation have been modified by a relatively homogeneous compressive strain (Ramsay 1967). Rare folds produced by slip on the cleavage planes were observed towards the south of the block (Plate 7E).

Fold train and fold stack inflection surfaces are shown in Figure 29 and values of Z have been calculated from the formula (p.20), and also measured from photographs (Table 4). Within one stack, with the exception of fold B, the ratio Z/L is remarkably consistent. The angle between the AS and the TIS is usually 90° whereas values for $\phi$ (SIS $\angle$ AS) range from 5°-31° (Fold A), 31°-56° (Fold B) and 4°-56° (Fold C) and hence approximate to those of certain layers of class 1 folds.

Using the grid for the classification of fold attitudes devised by Rickard (1971) the folds of the Coffs Harbour Sequence are upright to steeply inclined (Fig. 27B). Boudins have been observed on the limbs of mesoscopic folds at Arrawarra (GR 6324 2754) and Bare Point (GR 6427 3040). At McCauleys Headland an almost isoclinal fold occurs where stretching of the limbs has occurred with subsequent fracturing and parting of the competent bed.

## STRUCTURES PRODUCED BY THE SECOND DEFORMATION (D2)

### 1. Planar Structures ($S_2$)

The results of D2 in the Coffs Harbour Sequence are observed as isolated zones of flexures and kink bands mainly confined to pelitic lithologies. In rare cases the $S_1$ cleavage has been folded to produce chevron folds. Some axial surfaces of kink bands and chevron folds have become fractures, thus producing an axial surface crenulation cleavage ($S_2$). The spacings between the $S_2$ fracture surfaces range from 7 mm to 25 mm, but $S_2$ is not penetrative on the scale of the outcrop. $S_2$ is considered to have formed after the strain in the rock could no longer be taken up by buckling.

### 2. Linear Structures [$L(So \times S_2)$, $L(S_1 \times S_2)$]

Extremely rare lineations produced during D2 result from the intersection of So and $S_1$ with $S_2$ and are best developed on $S_1$ surfaces where they appear as closely-spaced striae.

### 3. Mesoscopic Folds

The style of D2 folds varies from slight flexures through kinks in $S_1$ to tight chevron folds (Plates 8, 9 and Fig. 32). Quartz veins have been introduced parallel to $S_1$ during or after D2 and tend to be concentrated in the hinges. Dilatation fissures similar to those illustrated by Ramsay (1967, Fig. 7·119) are filled by quartz. The D2 folds are generally asymmetrical and many are non-plane and non-cylindrical. They die out, merge or birfurcate in the axial direction and also in the profile plane (Plate 8E). Thus, the axial surfaces of adjacent folds are not always parallel and $S_2$ can be quite variable in attitude in some folds. Interlimb angles vary from open (149°-150°) for the flexures, to close (67°-72°) for the chevron folds.

In most cases the asymmetrical folds do not occur between parallel enveloping surfaces and hence cannot be termed periodic. Nevertheless on Plate 9 it is possible to apply the formulae for asymmetrical folds (pp.10-14) if the long limbs are disregarded and the folded surfaces between the three axial surface traces are analysed. For two layers the following results were derived.

| | c | s | l | θ | λ | A | C |
|---|---|---|---|---|---|---|---|
| Surface 1 | 0 | 8 mm | 12 mm | 62° | 10.8 mm | 3.6 mm | 0 |
| Surface 2 | 0.6 mm | 10 mm | 15 mm | 73° | 15.8 mm | 4.7 mm | 0.02 |

PLATE 8

D2 Mesoscopic Structures from the Coffs Harbour Block.

A. Portion of a kink band in the cleavage. Colour variation across the axial surface is due to uniform extinction of white mica aligned parallel to the cleavage plane on the left hand side of the AS. The kink band is cut by a later quartz vein. Unit A, Coramba Beds, S32562, magnification x 20, crossed nicols.

B. Kink band in a fine siltstone. Brooklana Beds, S32650, magnification x 20, plane polarised light.

C. Kink band in an highly-cleaved mudstone, with colour variation on opposite limbs due to uniform extinction of aligned white mica. Unit D, Coramba Beds, S32433, magnification x 50, crossed nicols.

D. Photomicrograph of fracturing along axial surface of a microscopic D2 fold similar in style to that illustrated in Plate 9. Quartz veins have been emplaced parallel to the cleavage planes and the fold is cut by younger quartz veins. Brooklana Beds, magnification x 25, crossed nicols.

E, F. Hand specimen slabs of box-type folds produced by conjugate kink bands in the cleavage. Brooklana Beds, Wild Cattle Creek Antimony mine area (GR 5815 2562), magnification x 1.

A

B

C

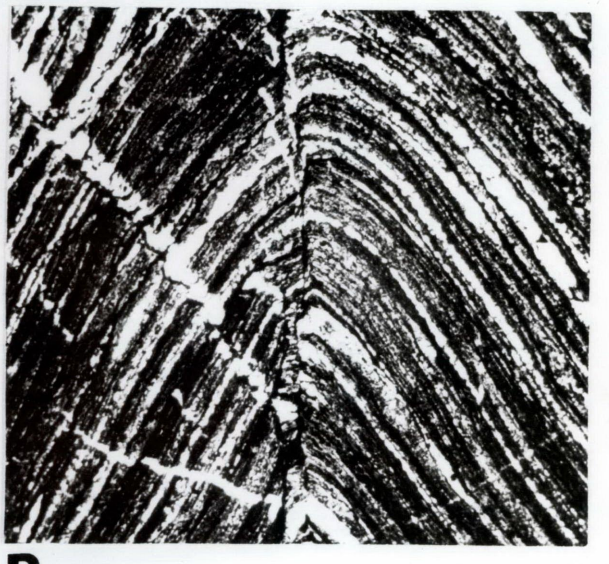

D

E

F

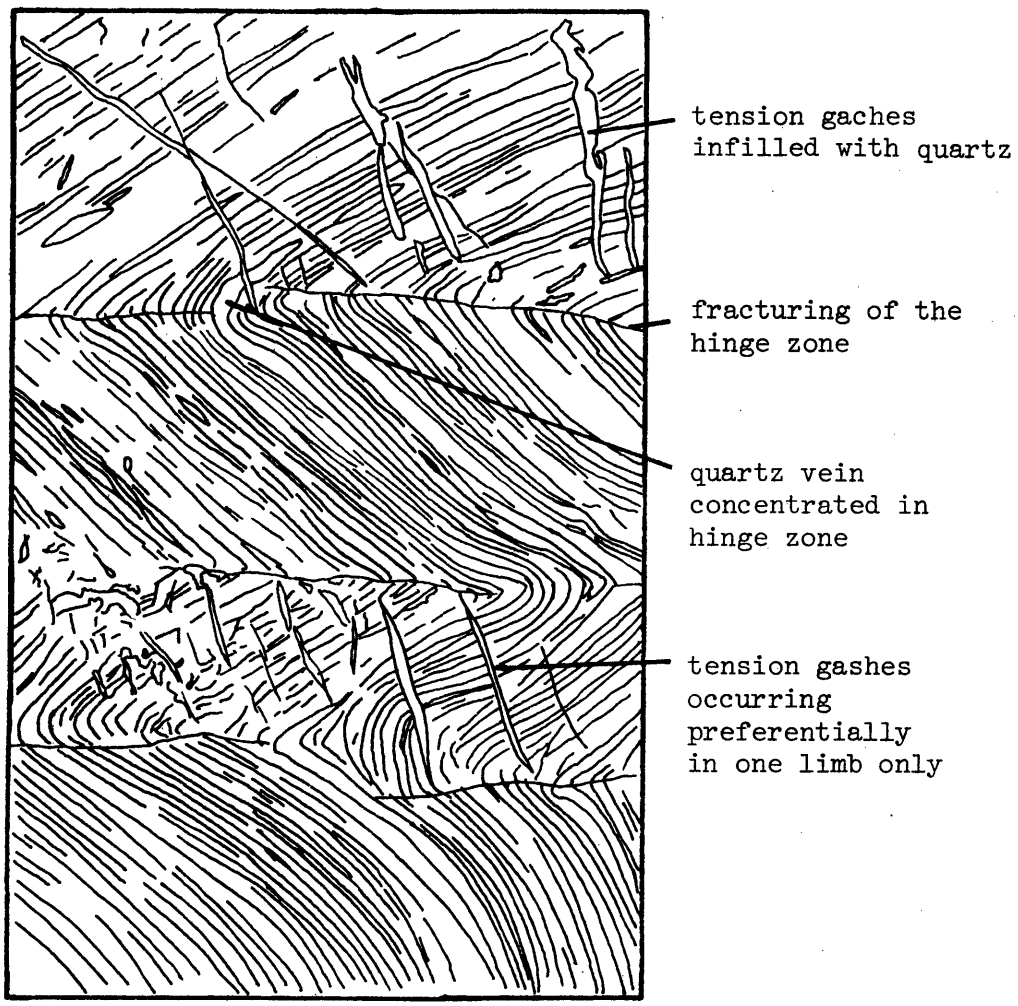


PLATE 9: D2 asymmetrical folds in $S_1$ cleavage. Quartz veins have been emplaced parallel to the cleavage and are often preferentially concentrated in the hinge zones as small saddle reefs. Specimen collected from Wild Cattle Creek mine area (GR 5815 2562). Brooklana Beds, magnification of photograph x 6.5.

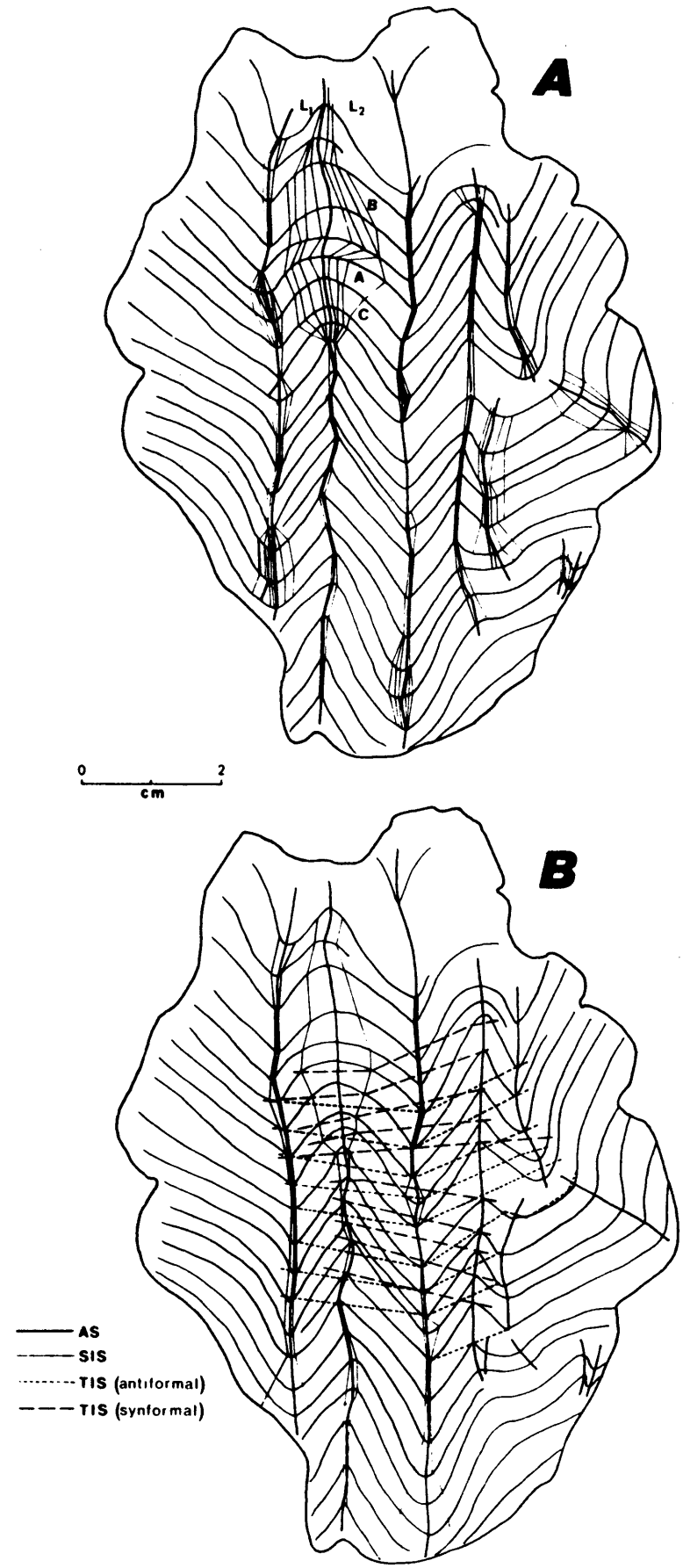


Fig. 32: Dip isogon (Fig. A) and inflection surface (Fig. B) patterns for a D2 mesoscopic fold from the Coffs Harbour Sequence.

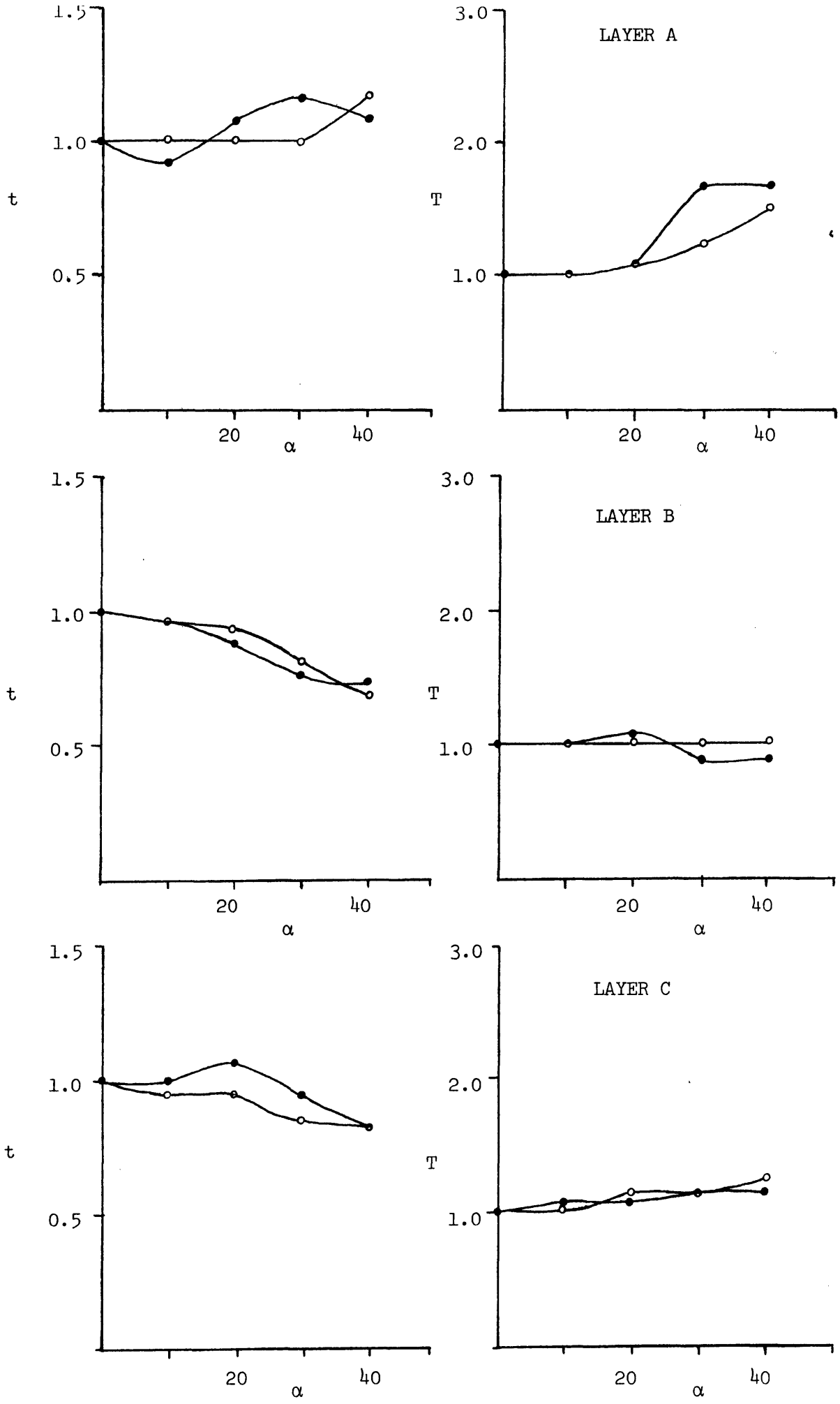


Fig. 33: T and t compared with α for the D2 fold from the Coffs Harbour Block. • = Limb 1, ° = Limb 2.

There is a close similarity between the dimensions of the two adjacent surfaces in the fold stack. For the non-periodic folds there is no truly characteristic $\lambda$ and A.

Dip isogons for several layers converge and diverge but more commonly are parallel to each other (Fig. 32A). Each layer shows the characteristics of several of the classes of Ramsay (1967) on a T and t versus $\phi$ graph (Fig. 33). Layer A contains features of classes 1A, 1B and 1C with class 1A dominant. Layer B contains features of classes 1C, 2 and 3, with class 2 dominant. Layer C is mainly in class 1C but elements of class 1A and 1B occur. However the majority of the layers have parallel isogons indicative of class 2.

Inflection surfaces (Fig. 32B) show that the SIS occur parallel to the AS and are almost coincident with them. This is typical of angular folds. The TIS are widely spaced and because of the asymmetry of the folds are not perpendicular to the AS. The angles range from 65° to 85°.

The tendency of the structures to die out, divide or birfurcate up and down the stack, and the non planar subparallel nature of the axial surfaces, indicate that shear along $S_2$ was not responsible for the formation of the folds. They probably resulted from the flattening of flexures induced by flexural-slip along the $S_1$ layering. During the flattening one limb of the fold illustrated in Plate 9 was extended in the direction of the cleavage opening up tension gashes which have been infilled with quartz. Fracturing in the hinge zone has also occurred for some of the layers.

Mesoscopic Faults

Numerous mesoscopic faults of variable strike occur throughout the Block. Displacements are both sinistral and dextral and range mostly from 0.03 m to 0.3 m. At a larger fault of attitude 079/N/50 at Signal Hill massive greywackes are thrust southwards over well bedded layers (Plate 10A). At Bare Point (GR 4323 3036) there is a series of mesoscopic faults, mainly thrusts. For faults in Figure 34A the original length of the marker horizon has been approximately 160 m and length of outcrop is now around 104 m - a shortening of almost 35%. In Figure 34B the original length of 24 m has been reduced to 19 m - an approximate shortening of 20%. Many microscopic faults were seen in thin section (e.g. Plate 10B).

PLATE 10

A. Massive greywacke unit thrust southward over well bedded layers at the headland of Signal Hill. Preferential erosion has occurred along the thrust plane. Photograph covers an area of approximately 7m x 7m.

B. Microscopic normal fault in an interbedded mudstone and siltstone. A strike-separation of 1.7mm has occurred. Unit D, Coramba Beds, S32403, magnification x 20, crossed nicols.

C. En echelon quartz veins emplaced in ac-joints and distorted to produce the sigmoidally folded tension gashes. Unit D, Coramba Beds, Arrawarra Headland. Photograph covers an area of approximately $1m^2$.

D. Ptygmatically folded quartz vein in a mudstone being cut by a network of planar quartz veins which appear to be emplaced later than the ptygmatic vein. Brooklana Beds, S32614, magnification x 20, plane polarised light.

E. Portion of a ptygmatically folded quartz vein in an interbedded siltstone and mudstone unit. Brooklana Beds, S32585, magnification x 50, plane polarised light.

F. Same fold as illustrated in Plate 10E but viewed under crossed nicols. Note elongate growth of quartz oriented subperpendicular to the folded surfaces of the vein.

A

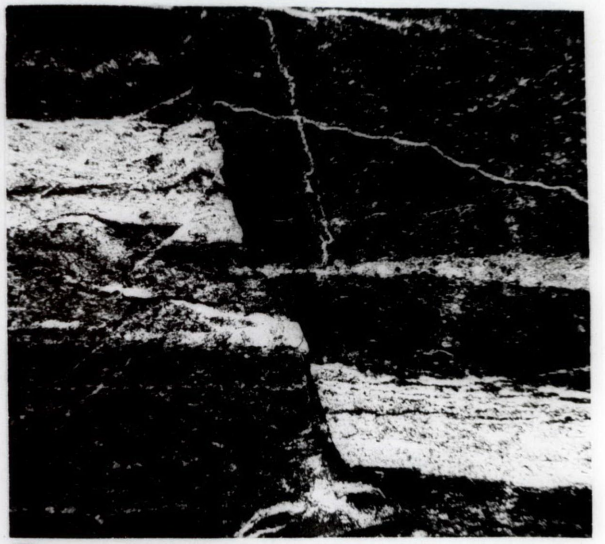

B

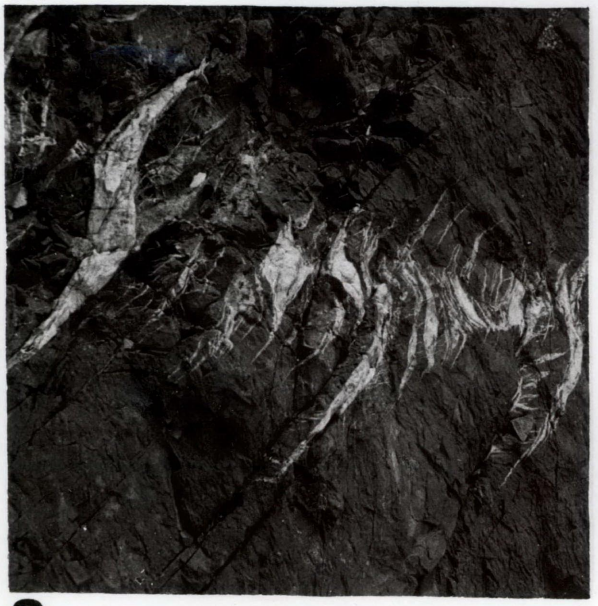

C

D

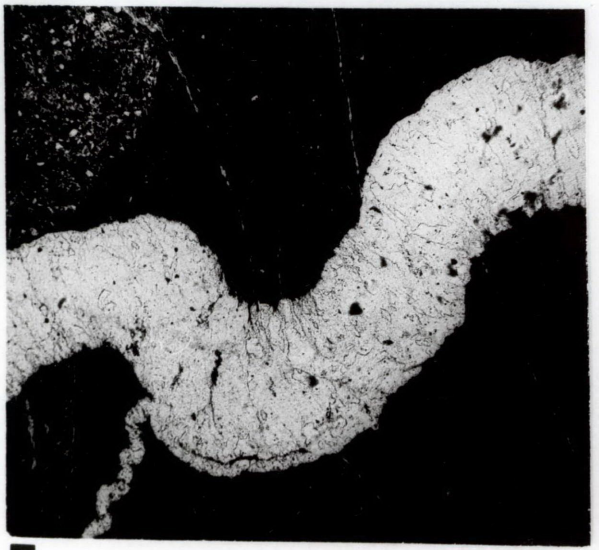

E

F

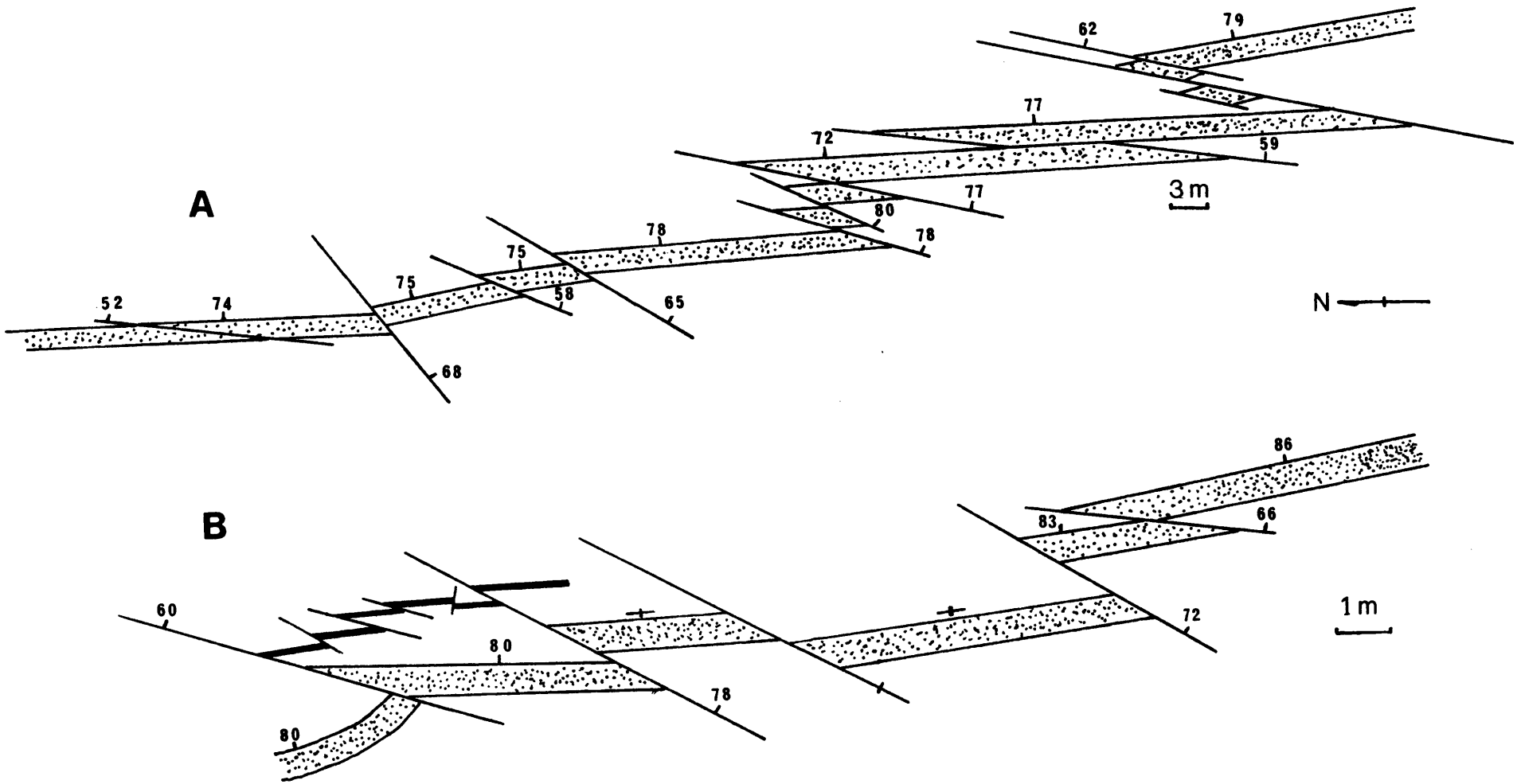


Fig. 34: Mesoscopic fault patterns from Bare Point.

Joints

Joints of many orientations are very common in the Coffs Harbour Sequence and at some localities the ac-set is readily recognised. No use has been made of joints in the structural analysis mainly because of their seemingly random pattern at many localities.

Quartz Veins

Numerous quartz veins occur in ac-joints and in en echelon arrangements, and some are ptygmatically folded. The en echelon veins may have formed in one of two ways:

(1) by simple shear deformation such as outlined by Ramsay (1967, pp.83-91), or

(2) by the opening up of rock material across the layers within a kinked zone because the layer thicknesses remain constant throughout the fold (Anderson 1964). The fissures are often filled with crystalline material to give dilatation veins.

In the Coffs Harbour Sequence sigmoidally folded quartz veins appear to have been formed by both processes. Plate 9 illustrates quartz veins formed in fissures in a kinked zone. The en echelon veins in Plate 10C are intimately associated with the ac-joints, and probably were produced by the first process.

Ptygmatic folds

Ptygmatic folds occur but are mainly confined to the southern part of the Coffs Harbour Sequence where deformation has been more intense. The best examples are observed at Boambee and Bonville headlands and typical styles are shown in Plate 10D-F. The ptygmatic veins appear to be the result of buckling of originally planar quartz veins.

## Macroscopic Structure

### INTRODUCTION

The presence of macroscopic structures in the Coffs Harbour Block has been inferred largely from changes in the orientation of mesoscopic structures and the distribution of the lithologic units (Map 1) and metamorphic zones (Map 2). Methods of structural analysis for the

macroscopic interpretation of the mesoscopic orientation data follow Turner and Weiss (1963) and Ramsay (1967). Most previous structural analyses have been attempted over small areas which are well exposed (see examples cited by Whitten 1966, pp.358-376). Here the structural analysis is attempted on an area of approximately 3,000 sq.km and problems have arisen because much of the region is poorly exposed, making it difficult for interpretation of macroscopic structures.

The Coffs Harbour Block has been subdivided into 24 domains homogeneous with respect to $S_1$. Where this foliation exhibits similar orientations between adjacent domains, the relevant domains were divided using the orientation of the D1 fold axes. Individual domains are outlined on Map 3.

The orientation of the mesoscopic structures are presented on equal-angle lower hemisphere stereographic projections (Wulff nets) for each domain (Fig. I, in Map Folder). Most of the stereographic projections have been plotted using computer program WULFF which automatically contours the data (see Appendix II). The use of contoured stereographic projections rather than the conventional equal area (Schmidt or Lambert) projections needs justification. Several nets contoured by the squared-grid method (Stauffer 1966) on equal area projections by Korsch (1968) were duplicated using program WULFF. Good reproducibility occurred and it is considered that minor differences were not significant enough to outweigh the enormous decrease in the amount of time required to prepare the nets.

Stauffer (1966) considers a minimum of 100 points are needed to justify contouring to determine a statistical pattern. Nevertheless Stauffer and Mukherjee (1971) present equal area Π-plots where nets with as low as 13 points have boundary lines drawn by "eye" to indicate areas of low and high density. For this study nets with as few as 10 points have been contoured by WULFF. Two factors influenced their use: (a) the time saved by computer plotting over manual methods, and (b) preliminary plots indicated that the detailed density counts help to delineate accurately the position of the point maxima or girdle.

A summary of data from the various domains is presented in Table 5. The stereographic projections indicate some aspects of the geometry of the macroscopic structures but not scale or location which are shown on the idealised trend line maps for So and $S_1$ (Maps 4 and 5). Because of the irregular distribution of the sampling points and large amounts of data from small areas of good exposure, the maxima for So and $S_1$ orientations

Table 5: Summary of geometry of elements from the macroscopic domains in the Coffs Harbour Block, stereographic projections for each element are included in the map folder.

| Domain | ΠSo | $\Pi S_1$ | L(So x $S_1$) | $B^{S_1}_{So}$ | ΠAS(So x $S_1$) | $B^{S_2}_{So}$, $B^{S_2}_{S_1}$ | ΠAS(So x $S_2$, $S_1$ x $S_2$) |
|---|---|---|---|---|---|---|---|
| 1 | point maxima at 2 to 034 defines plane 124/S/88 | point maxima at 4 to 047 defines plane 137/SW/86 | great circle girdle 144/SW/82 | - | - | - | - |
| 2 | partial girdle of 025/E/82 β = 8 to 295 | point maxima at 8 to 028 defines plane 118/S/82 | two points, average 40 to 135 | one point 26 to 080 | one point 076/ S/64 | three points, average 20 to 095 | three points, average 090/ S/59, all dextral kinks |
| 3 | point maxima at 12 to 009 defines plane 099/S/78 | point maxima at 22 to 020 defines plane 110/S/68 | great circle girdle 112/S/75 | two points, average 36 to 190 | two points, average 003/W/78 | - | one point 350/E/08, sinistral kink |
| 4 | partial girdle of 036/NW/80 β = 10 to 126 | point maxima at 12 to 039 defines plane 129/S/78 | great circle girdle 132/SW/75 | two points, average 56 to 294 | two readings, average 166/W/63 | - | - |
| 5 | point maxima at 1 to 009 defines plane 099/S/89 | point maxima at 11 to 022 defines plane 112/S/79 | partial great circle girdle 104/S/78 | two readings, average 34 to 096 | two readings, average 147/N/48 | - | three readings, average strike 028, variable dip |
| 6 | point maxima at 9 to 009 defines plane 099/S/81 | point maxima at 3 to 020 defines plane 110/S/87 | partial great circle girdle 098/S/75 | two readings, lie in E-W sub-vertical plane | one reading, 064/NW/74 | - | - |
| 7 | point maxima at 4 to 357 defines plane 087/S/86 | point maxima at 12 to 020 defines plane 110/S/78 | three points, average 75 to 252 | - | - | weak point maxima at 62 to 159 | possible great circle strike 110°, sub-vertical dip |
| 8 | point maxima at 12 to 004 defines plane 094/S/78 | point maxima at 5 to 023 defines plane 113/S/85 | partial great circle girdle 097/S/78 | three readings, lie in average S1 plane | three readings fall in the ΠS1 field | - | - |

Table 5: (continued)

| Domain | $\Pi_{So}$ | $\Pi_{S_1}$ | $L(So \times S_1)$ | $B^{S_1}_{So}$ | $\Pi AS(So \times S_1)$ | $B^{S_2}_{So}$, $B^{S_2}_{S_1}$ | $\Pi AS(SoxS_2, S_1xS_2)$ |
|---|---|---|---|---|---|---|---|
| 9 | point maxima at 12 to 360 defines plane 090/S/78 | point maxima at 6 to 010 defines plane 100/S/84 | partial great circle girdle 091/S/82 | - | - | - | - |
| 10 | point maxima at 6 to 340 defines plane 070/S/84 | point maxima at 4 to 008 defines plane 098/S/86 | scatter with strongest cluster around 67 to 090 | - | - | - | - |
| 11 | point maxima at 15 to 174 defines plane 084/N/75 | point maxima at 3 to 351 defines plane 081/S/87 | scatter with strongest cluster around 38 to 290 | - | - | - | - |
| 12 | point maxima at 16 to 196 defines plane 106/N/74 | point maxima at 11 to 202 defines plane 112/N/79 | great circle girdle 113/NE/82 | point maxima at approximately 70 to 134 | variable strikes but all steeply plunging | dextal kinks point maxima 31 to 120 sinistral 71 to 038 | random pattern |
| 13 | point maxima at 7 to 003 defines plane 093/S/83 | point maxima at 3 to 192 defines plane 102/N/87 | great circle girdle 100/N/86 | point maxima 56 to 098 | average plane 104/vertical | dextral kinks gently plunging to east and west | average plane 095/S/30 |
| 14 | great circle girdle 041/S/26 $\beta$ = 64 to 311 | point maxima at 4 to 199 defines plane 109/N/86 | great circle girdle 103/N/80 | great circle girdle 106/vertical | scatter with densest concentration at 6 to 190 | - | three readings |
| 15 | random scatter with densest concentration at 124/N/88 | point maxima at 1 to 010 defines plane 100/S/89 | great circle girdle 110/N/84 | point maxima with subvertical plunges | one reading 118/N/88 | one point for dextral kink 80 to 280 | - |
| 16 | elongate point maxima at 9 to 171, plane 081/N/81 | point maxima at 9 to 170 defines plane 080/N/81 | great circle girdle 082/N/80 | great circle girdle similar to $L(S_o \times S_1)$ | - | - | - |

Table 5: (continued)

| Domain | $\Pi So$ | $\Pi S_1$ | $L(So \times S_1)$ | $B^{S_1}_{So}$ | $\Pi AS(So \times S_1)$ | $B^{S_2}_{So}$, $B^{S_2}_{S_1}$ | $\Pi AS(SoxS_2, S_1xS_2)$ |
|---|---|---|---|---|---|---|---|
| 17 | great circle girdle 187/E/75 $\beta$ = 15 to 277 | point maxima at 7 to 185 defines plane 095/N/83 | partial great circle girdle 096/N/75 | partial great circle girdle similar to $L(S_o \times S_1)$ | average plane strikes 094 with subvertical dips | one reading for dextral kink 73 to 029 | one reading 047/SE/76 |
| 18 | great circle girdle 162/W/40 $\beta$ = 50 to 072 | point maxima at 12 to 173 defines plane 083/N/78 | partial great circle girdle 086/N/70 | elongated point maxima 67 to 078 | one reading 076/N/88 | - | - |
| 19 | great circle girdle 162/E/80 $\beta$ = 10 to 252 | point maxima at 8 to 168 defines plane 078/N/82 | partial great circle girdle 075/N/75 | gently plunging to 070 and 240 | - | - | one reading 027/NW/74 |
| 20 | great circle girdle 076/N/75 $\beta$ = 15 to 166 | point maxima at 10 to 270 defines plane 000/E/80 | great circle girdle 174/E/70 | partial great circle girdle 197/E/50 | random pattern | dextral kinks plunge to SE; sinistral kinks:possible girdle? | dextral kink - NW-SE strike, sinistral kink NE-SW strike |
| 21 | point maxima at 16 to 265 defines plane 355/E/74 | point maxima at 22 to 288 defines plane 018/E/68 | great circle girdle 193/E/72 | partial great circle girdle 169/E/66 | subvertical dips, random strikes | dextral kinks plunge to S & SE, sinistral kinks plunge to NE | all kinks steeply dipping |
| 22 | great circle girdle 120/NE/75 $\beta$ = 15 to 210 | point maxima at 5 to 301 defines plane 031/E/85 | great circle girdle 215/E/70 | partial great circle girdle 196/W/85 | point maxima at 8 to 294 defines plane 024/E/82 | two dextral kinks | three dextral kinks |
| 23 | elongated point maxima or partial great circle | point maxima at 13 to 112 defines plane 022/W/77 | great circle girdle 194/W/80 | scatter with point maxima at 48 to 356 | subvertical dips, random strikes | two readings, average 80 to 336 | two readings, average 148/SW/87 |
| 24 | great circle girdle 115/S/75 $\beta$ = 15 to 025 | great circle girdle 122/S/85 $\beta$ = 5 to 032 | partial great circle girdle 223/W/84 | partial great circle girdle 020/W/70 | point maxima at 8 to 284 defines plane 014/E/82 | - | - |

on the stereographic projections do not always correspond with those observed on the trend line maps.

## ORIENTATION AND DISTRIBUTION OF D1 STRUCTURES

The only widely developed mesoscopic structures in the Coffs Harbour Block are So and $S_1$. Towards the southern parts of the Block, particularly in inland exposures, So is not seen nearly as commonly as $S_1$ and consequently D1 mesoscopic folds and L(So x $S_1$) are extremely rare. Hence for the inland domains (1-11) most of the data (excepting for $S_1$) have been collected in the northern parts where So is more readily observable. To simplify the discussion of macroscopic structure, domains have been grouped into two subdivisions separated by the Redbank River Beds.

### (1) SUBDIVISION 1 (Domains 1-19)

Within each domain $S_1$ is homogeneous forming point maxima. Variations in strike from 137° (Domain 1) to 078° (Domain 19) indicate a general progressive change from west to east across the Block with few exceptions (e.g. Domains 4, 12). Dips of $S_1$ are very steep either to the north or to the south and can be in both directions within one outcrop.

So exhibits point maxima defining modal planes in several domains with orientations slightly different from that of $S_1$. Strikes range from 124° (Domain 1) to 070° (Domain 10) and dips are very steep to both the north and south. Except in mesoscopic folds in some headlands the sedimentary structures all indicate that bedding faces to the north and hence south dipping beds from inland domains are overturned. Some domains have $\pi$So defining a great-circle girdle, and the $\beta$So axis so produced is coincident with $B_{So}^{S_1}$ (e.g. Domains 17, 18) indicating that for the D1 deformation $\beta So = B_{So}^{S_1}$. Where $\pi$So forms a girdle and $\beta = B$ then So has been deformed by plane cylindrical folding.

During D1 So was folded about horizontally to steeply plunging axes trending to the east or west. The irregular great circle arcs defined for So for several domains suggest that the fold axes have not been entirely parallel in any one domain. This may be inferred also from the standard deviations of plunges about the means (Fig. 35). For all domains in this subdivision, except Domain 14, the $B_{So}^{S_1}$ axes have consistent trends being either to the east or west but not both. The $B_{So}^{S_1}$ data from Domain 14 can be subdivided into two point maxima, one at 75 to 108 and the other at 70 to 304,

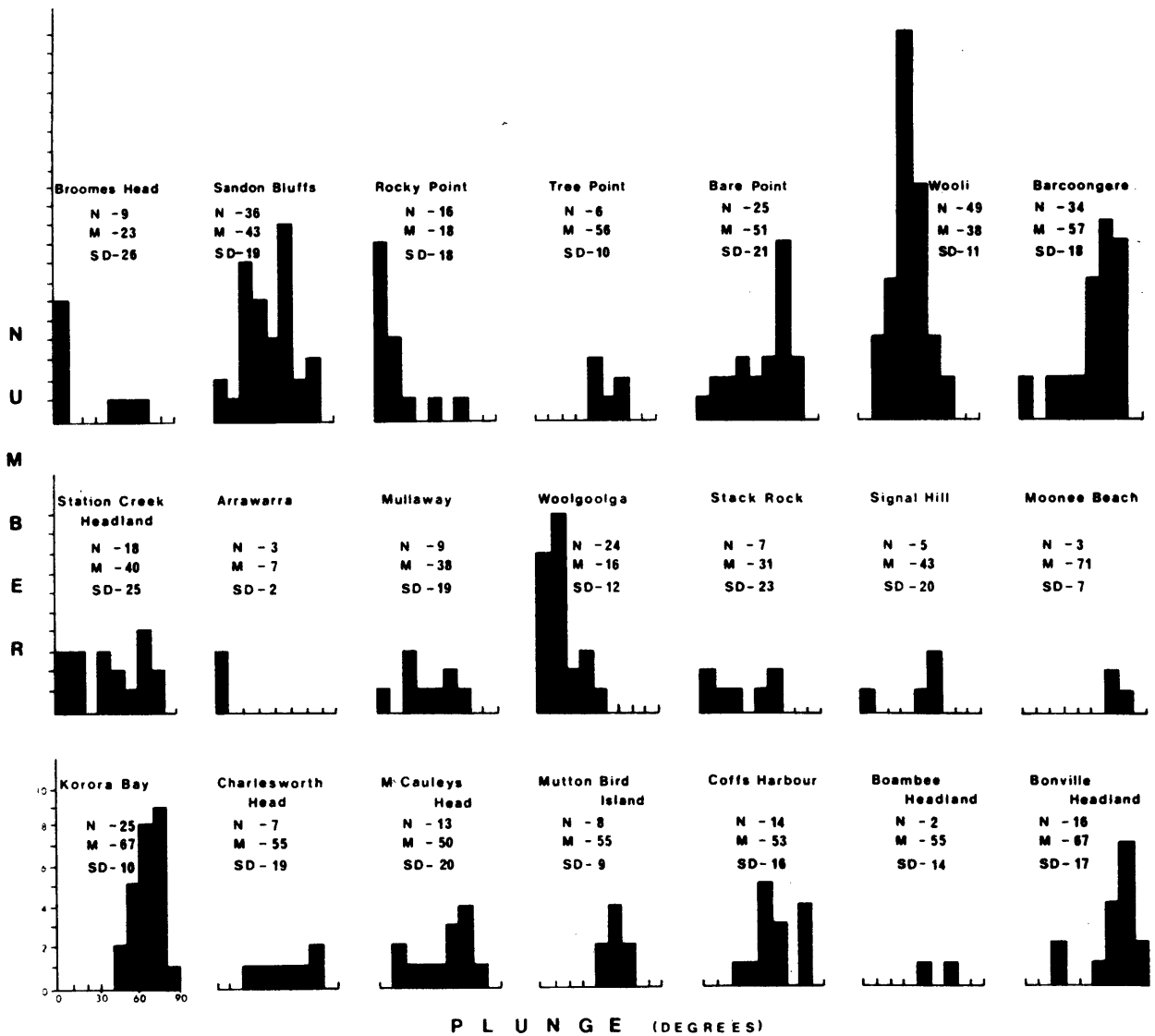


Fig. 35: Histograms for plunges of fold axes for mesoscopic folds observed on coastal headlands in the Coffs Harbour Block.

but it has not been possible to spatially subdivide this domain into distinct areas for the two point maxima.

D1 lineations [L(So x $S_1$)] for many domains define a great circle which varies in orientation from 144/SW/82 (Domain 1) to 075/N/75 (Domain 19). This girdle is parallel to the modal plane of the cleavage within individual domains and shows that the lineations lie in the cleavage plane. This plane is statistically the axial plane of the mesoscopic folds, and therefore L(So x $S_1$) = $B_{So}^{S_1}$.

(2) SUBDIVISION 2 (Domains 20-24)

Most data from this subdivision have been collected from the well exposed rocks of the coastal headlands. Within each domain $S_1$ is homogeneous defining a point maximum. Average strikes range from 000° to 049° and dips are always steep, usually greater than 75°, with dip directions to both the east and west. The cleavage is mainly a fracture cleavage.

So nets define either point maxima (e.g. Domains 21, 22) or girdles (e.g. Domains 20, 24). Where point maxima occur the average strike ranges from 355° to 037° with dips usually steep. In domains 20-22 the average dip of bedding is steeply to the west (about 70°-75°) whereas for domains 23 and 24 the average dip is steeply to the east (about 60°-65°). All sedimentary structures providing facing evidence indicate that the sequence faces to the west, and that beds which dip to the east are overturned. For domains where ΠSo define a great circle the $\beta_{So}$ axis is coincident with some of $B_{So}^{S_1}$ suggesting that $\beta_{So} = B_{So}^{S_1}$, and So has been deformed by plane cylindrical folding.

So was folded about horizontal to steeply plunging fold axes ($B_{So}^{S_1}$) trending either to the north or to the south, e.g. fold axes from Domain 21 plunge to the north whereas those from Domain 20 plunge to the south. Changes in the plunge of the fold axes and interlimb angles are discussed later. The irregular great circles defined by ΠSo indicate that the fold axes have not been entirely parallel during D1 deformation, a conclusion that is supported by the variation in plunges of fold axes at various headlands (Fig. 35).

All $B_{So}^{S_1}$ axes lie in or very close to the modal plane of the cleavage for each domain indicating that the cleavage has an axial plane relationship with the folds produced by D1. L(So x $S_1$) lineations define great circle girdles ranging in orientation from 174/E/70 to 223/W/84. Several explanations are offered below for the formation of a girdle for L(So x $S_1$).

Possible reasons for formation of an L(So x $S_1$) girdle

It is difficult to explain the L(So x $S_1$) girdle in some domains, particularly where So and $S_1$ occur as point maxima. A point maxima for So may be explained by one of three possible alternatives:

(a) The sequence is a monotonous uniform depositional sequence which is not repeated by any structural mechanism. The presence of mesoscopic folds and cleavage negates this suggestion.

(b) The strate are repeated several times by isoclinal folding. This would also explain the parallelism of bedding and cleavage observed throughout the sequence. No evidence of isoclinal folds was found and all facing evidence indicates that the sequence youngs consistently in one direction.

(c) The sequence has been cut by thrust faults parallel or subparallel to bedding (e.g. Lillie 1963, Fig. 5). This would tend to thicken the sequence but maintain the constant orientation. The parallelism of So and $S_1$ would be explained by possibly one macroscopic fold for the whole region.

Four possible reasons for the L(So x $S_1$) girdle are:

(1) Most L(So x $S_1$) have been determined by the intersection on a stereographic projection of accurate measurements of both So and $S_1$ from the same very small area. β-points become spurious when the angle between So and $S_1$ becomes extreme (less than 40° or greater than 140°) and hence the error of measurement is large (Ramsay 1964). For example an So of 124/S/88 and $S_1$ of 137/S/86 (average planes from Domain 1) intersect at an angle of 13°. Assuming an order of accuracy for the field measurements of 5°, then by substitution into the formula of Ramsay (1967, p.14) the maximum error for the β-intersection is 50.4°.

When all β-intersections are plotted for one domain they might define a zone for the maximum errors which is similar to the girdles seen in Figure I (in Map Folder). However Korsch (1968, Fig. 67) showed that for individual small areas within the Woolgoolga district there was a high correlation between the nets of $B_{So}^{S_1}$ and L(So x $S_1$) and hence this reason is possibly invalid.

(2) The L(So x $S_1$) girdle might be explained by the deformation of a non-planar So-surface. Then the D1 deformation would have been preceded by an earlier deformation of So, which might have been either a tectonic or a soft sediment deformation. Although areas of soft sediment deformation are present in the Coffs Harbour Sequence (see Appendix I, p.34) it is considered that the majority of the Sequence has not been influenced by large scale slumping and consequently this explanation is invalid.

(3) The L(So x $S_1$) girdle might have resulted from a later deformation which produced similar folds and spread the lineations along a great circle. If this occurred some deformation of $S_1$ might also be excepted However the $\pi S_1$ exhibit point maxima for every domain and hence $S_1$ has not been deformed subsequent to formation. It would require a stress field of a very particular and unusual orientation to produce a deformation where a plane would appear to remain undeformed while a lineation in the plane is itself deformed. The only evidence for a later mesoscopic deformation is the infrequent development of kink and chevron folds on a small scale the distribution of which cannot be related to areas where L(So x $S_1$) define a girdle. Hence this possible reason is invalid.

(4) It has already been shown that when two planes intersect each other it is possible to have a large change in the plunge of the resultant lineation with only a small change in the strike and dip of the intersecting surfaces (p.24). Therefore only small changes in the strike and dip of So and $S_1$ might result in large changes in the resultant plunge of L(So x $S_1$), which might provide the observed girdles. While $\pi S_1$ appears to be statistically homogeneous within one domain, the spread of the points about the point maxima indicates strike differences of up to 40° and variations in dip of up to 20° occur. Coupled with the variations in strike and dip for So within the same domain, it appears likely that variations in the plunge of lineations will result. This hypothesis is favoured over other alternatives.

Progressive change in the intensity of D1 deformation

In the southern portion of the Coffs Harbour Sequence there is a progressive change from north to south in the plunge of the fold axes from subhorizontal to steeply plunging and associated with this the interlimb angles change from open to tight, indicating a progressive increase in the

intensity of the D1 deformation towards the south (Fig. 37A). Only data from the well exposed coastal headlands (Domains 12-24) are included here, because of the absence of significant amounts of data from the more poorly exposed inland outcrops. The data have been processed by computer programs SORTILA and PLUNGEFA (see Appendix II) and the results graphed in Figures 35 and 36. The relationship between the interlimb angle and dip of bedding and plunge of fold axes is shown in Figures 37B and C.

Subdivision 1: The change in the plunge of fold axes with increasing deformation might be explained by the model where an originally horizontal bed is being deformed and a nearly vertical axial surface is developing (pp.21-25 and Figs. 10-12). It has been shown possible to have a simple geometric relationship where the plunge of the fold axes changes progressively while the dip of the axial surface remains constant. However the strike of the marker horizon and the strike of the axial plane must not be the same (p.24). The strikes of bedding and cleavage for the various domains are never the same but differ by a few degrees (usually 6°-24°) between average planes of So and $S_1$ (Fig. I and Table 5).

Another explanation to produce the change in plunge of fold axes from north to south assumes that the folds originally had the same plunge. Now if the Demon and Bellinger Faults formed the one continuous curved thrust plane then thrusting of the Coffs Harbour Sequence up this curved surface could produce the required orientations. Because of tectonic implications this hypothesis will be dealt with in Section II.

In general, a small interlimb angle can be correlated with a steep dip in bedding (Fig. 37C). The theoretical line on this diagram is for an originally horizontal marker bed being folded to produce angular folds and finally producing isoclinal folds with the dip of the limbs being vertical.

The decrease in the intensity of deformation towards the north might be related possibly to a fold model devised by Willis (1893) and developed further by Johnson (1970). In his zone of open folds from the Appalachian Mountains Willis found that the folds were more oppressed in the east than in the west. He explained this by a driving force applied at the eastern edge of the stack of layers which was transferred towards the west partly through the relatively incompetent substrata. Willis and Willis (1929) performed a series of activities using an horizontal force to buckle a series of layers in an attempt to reproduce experimentally the Appalachian folds.

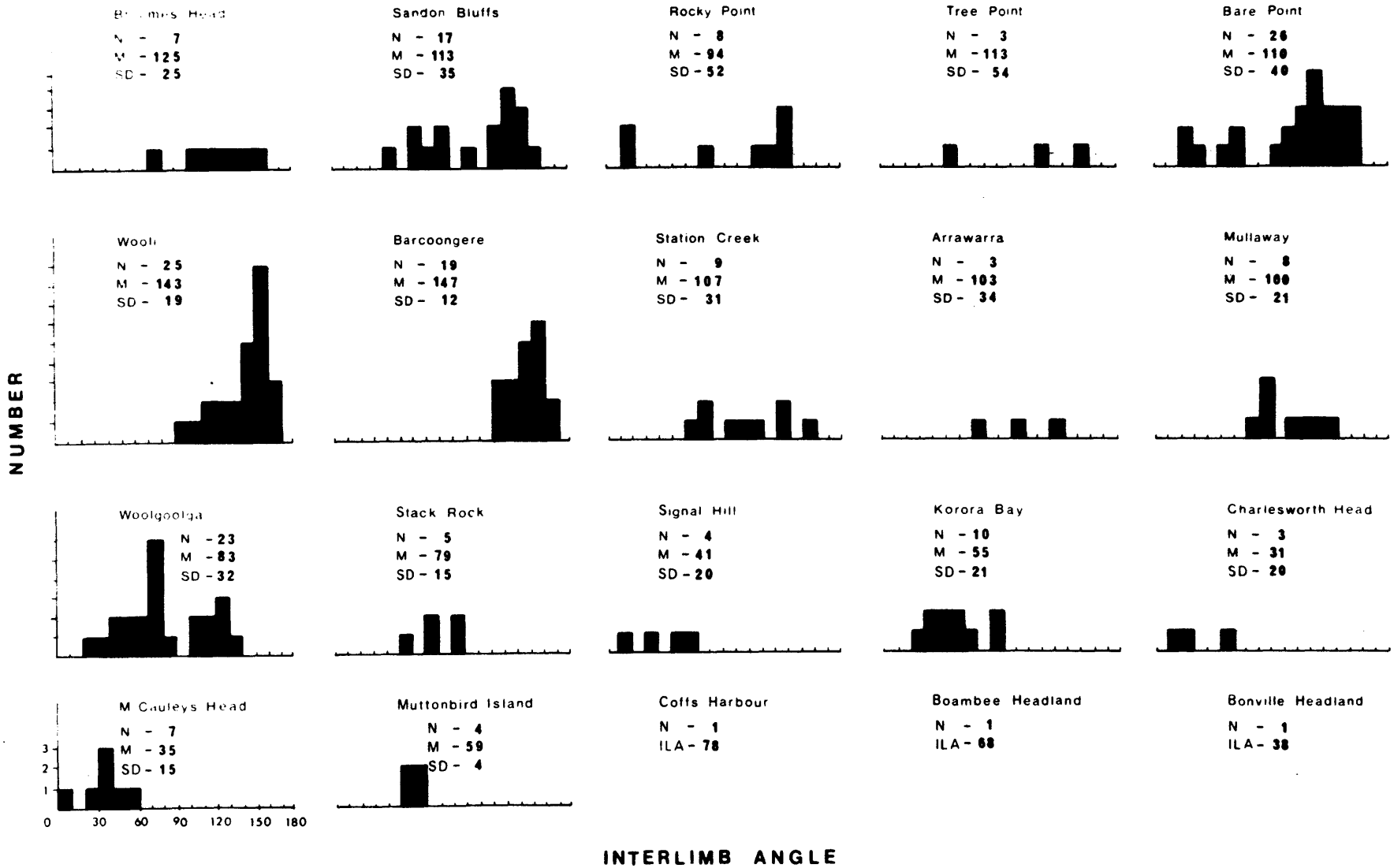


Fig. 36: Histograms of interlimb angles for mesoscopic folds observed at coastal headlands in the Coffs Harbour Block.

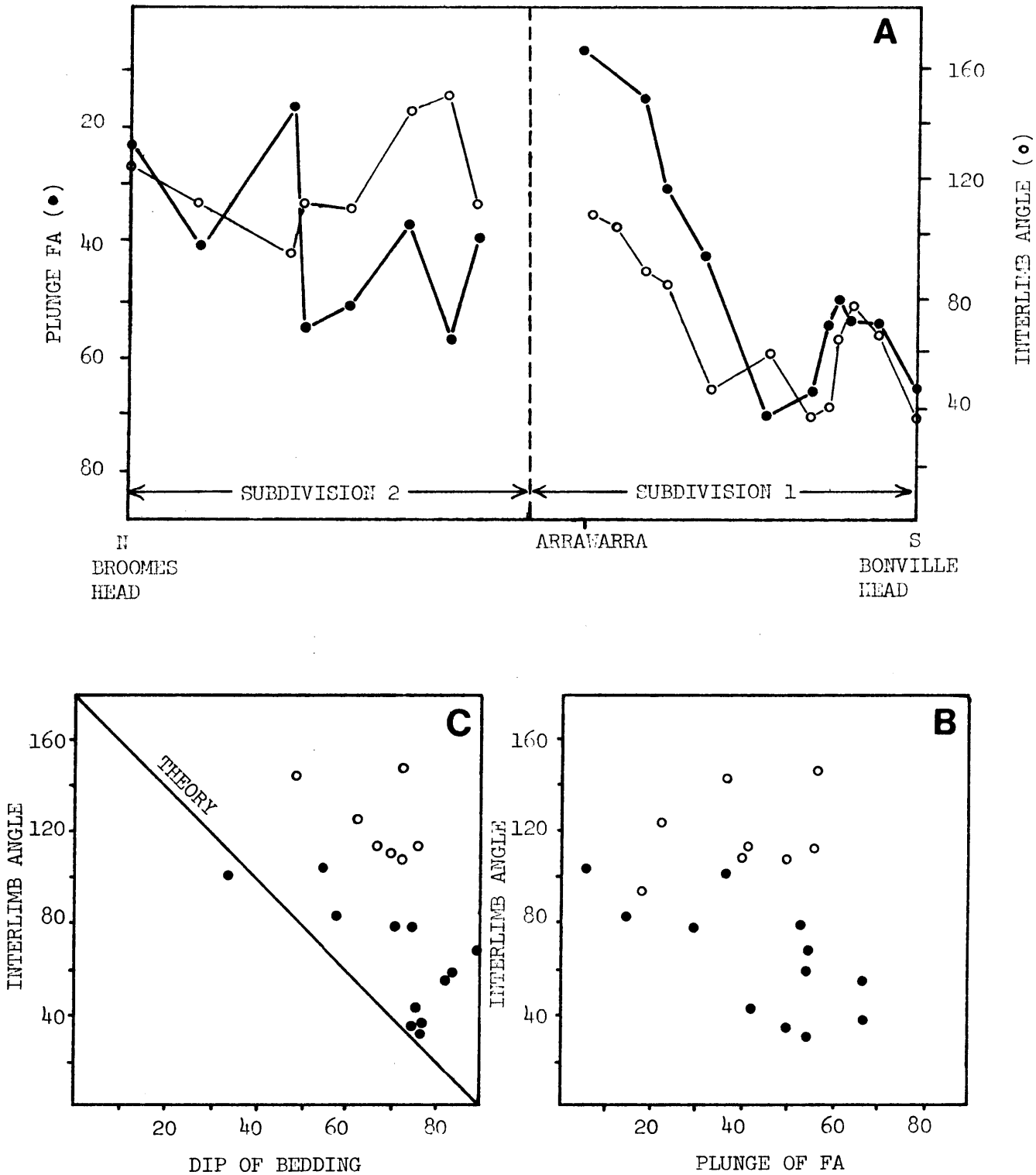


Fig. 37: Relationships between interlimb angles, plunge of fold axes, dip of associated bedding and the change over the distance south from Broomes Head towards Bonville Head.

In Figs B and C • = Subdivision 1, o = Subdivision 2.
For full explanation see text.

Johnson (1970) showed that a train of folds can be predicted by mathematical theory. Equation 3-30 of Johnson (1970, p.96) defines a sine curve where the wavelengths of the theoretical folds are constant but the amplitudes diminish with increasing distances from the applied axial load.

Consequently the folds from the Coffs Harbour Sequence are considered to have formed possibly as the result of an axial load which was horizontal and was directed from the south. Mechanisms, such as the Coffs Harbour Block being buttressed by rocks from the Nambucca Slate Belt or the Coffs Harbour Block being forced against a stable Nambucca Slate Belt, will be discussed in Section II.

Subdivision 2: A simple progressive change in one direction similar to that of Subdivision 1 does not occur (Figs. 35-37) and little correlation between the interlimb angle and dip of bedding and plunge of fold axes can be seen. If there has been any rotation of this northern subdivision then the plunges and dips might have been originally less than their present amount. Hence the only variable which would not be affected would be the interlimb angle. Interlimb angles from this subdivision are similar to or larger than those from Arrawarra and Mullaway possibly suggesting that this subdivision was located to the east and slightly north of Arrawarra prior to the suggested rotation.

### Possibility of D1 macroscopic structures

It has not been possible to delineate any macroscopic structures produced by D1 apart from the steepening in the orientation of the bedding. However any macroscopic fold might have been obliterated by subsequent macroscopic folding and faulting during D3 deformation.

## ORIENTATION AND DISTRIBUTION OF D2 MESOSCOPIC STRUCTURES

Mesoscopic structures produced by D2 are kink folds and chevron folds in the $S_1$ cleavage and occur only in isolated areas throughout the Coffs Harbour Sequence. Orientations of the structures are shown in Figure I (in Map Folder) and summarised in Table 5. Both dextral and sinistral kinks occur but it was not possible to delineate any macroscopic structure using the vergence of the kink folds to indicate which limb of a macroscopic fold they were located on.

Because of the limited amount of data available, differences between individual domains could not be recognised with any confidence and hence

composite plots for dextral and sinistral kinks have been compiled for the two subdivisions (Fig. 38). In general the structures from subdivision 1 define girdles which are approximately east-west in strike. This contrasts with those from subdivision 2 which have a north-south or northeast-southwest strike. Due to the infrequent occurrence of D2 structures in the Coffs Harbour Sequence it was not possible to define any macroscopic structure associated with this deformation.

Warping of bedding and cleavage

An explanation of the gentle warping of the bedding and cleavage throughout the Block (see Maps 4, 5 and Fig. I) producing slight changes in the orientation of the s-surfaces must also explain how the steeply dipping beds often became overturned. Several alternatives are:

(a) A series of isoclinal folds which produce slight variations in the orientation of So and $S_1$ (Fig. 39A). However no evidence for isoclinal folds has been found over large areas and hence this suggestion is possibly invalid.

(b) The monotonous sequence has been slightly deformed due to drag along the faults illustrated on Map 1. The movements might result in slight twisting and drag of the sediments between two faults, particularly if there has been any rotational component of movement along the faults. The beds might be deformed from an originally parallel sequence into one which dips steeply to the north or to the south but youngs in one direction only (Fig. 39B).

(c) The point maxima defined by the stereographic projections are only statistical maximum densities resulting from a spread of orientations which, due to the natural inhomogeneous nature of rock, were not perfectly parallel, and later deformation by D1 or D2 has enhanced the differences in strike and dip of the beds.

(d) The warping might be the result of a series of thrust faults with only small displacements. Because the thrusts would parallel the strike of the beds they would be extremely difficult to locate. Only one such fault has been found at Signal Hill (GR 6308 2616) where a thick massive greywacke unit has been thrust over a well bedded sequence which has been slightly deformed by drag along the thrust. The patterns possibly produced by this mechanism (Fig. 39C) would explain slight changes in strike as well as changes in dip from north to south without a change in the facing direction. This mechanism is preferred over other alternatives.

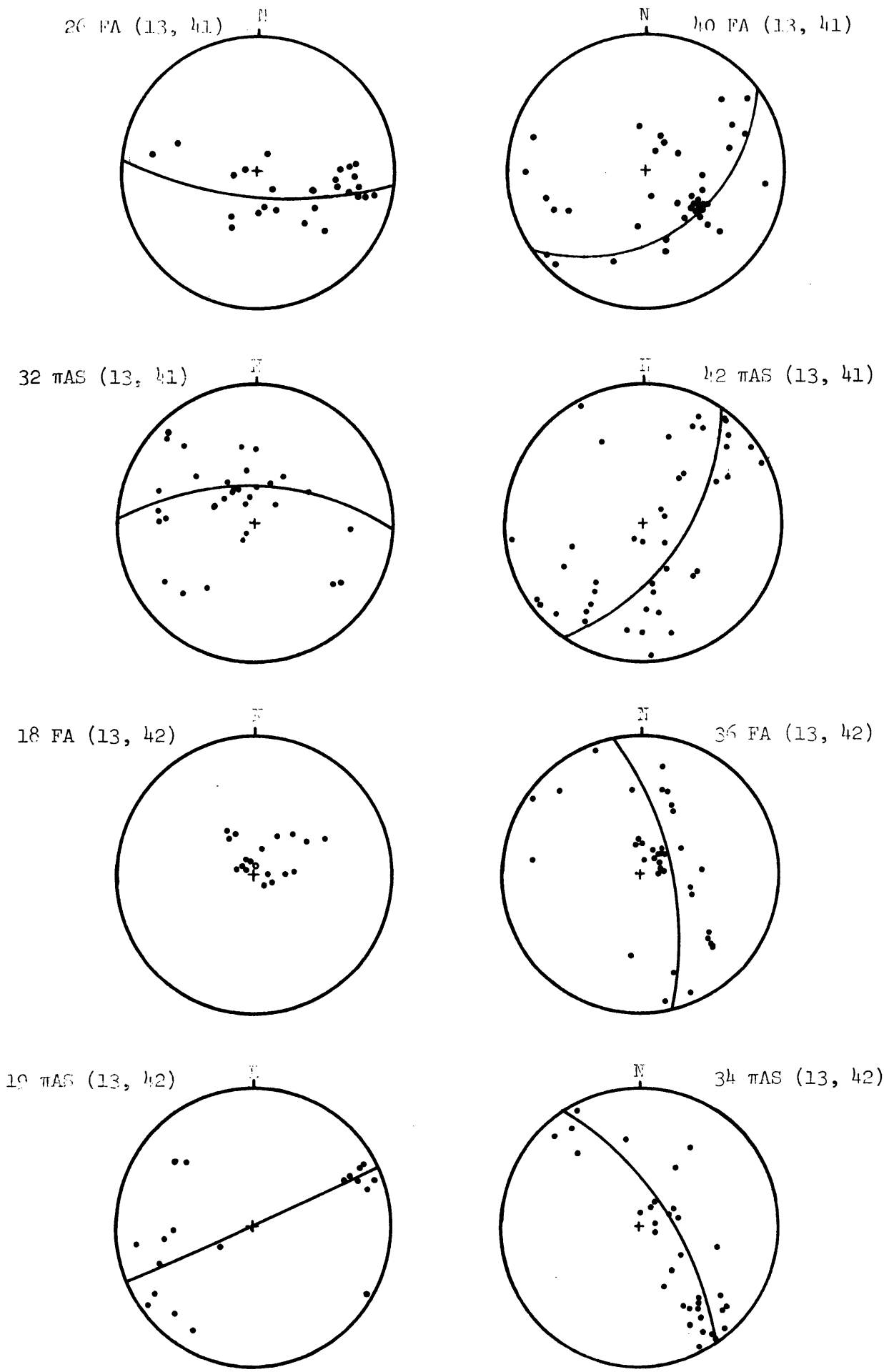


Fig. 38: Stereographic projections for kink bands from the two subdivisions of the Coffs Harbour Block.

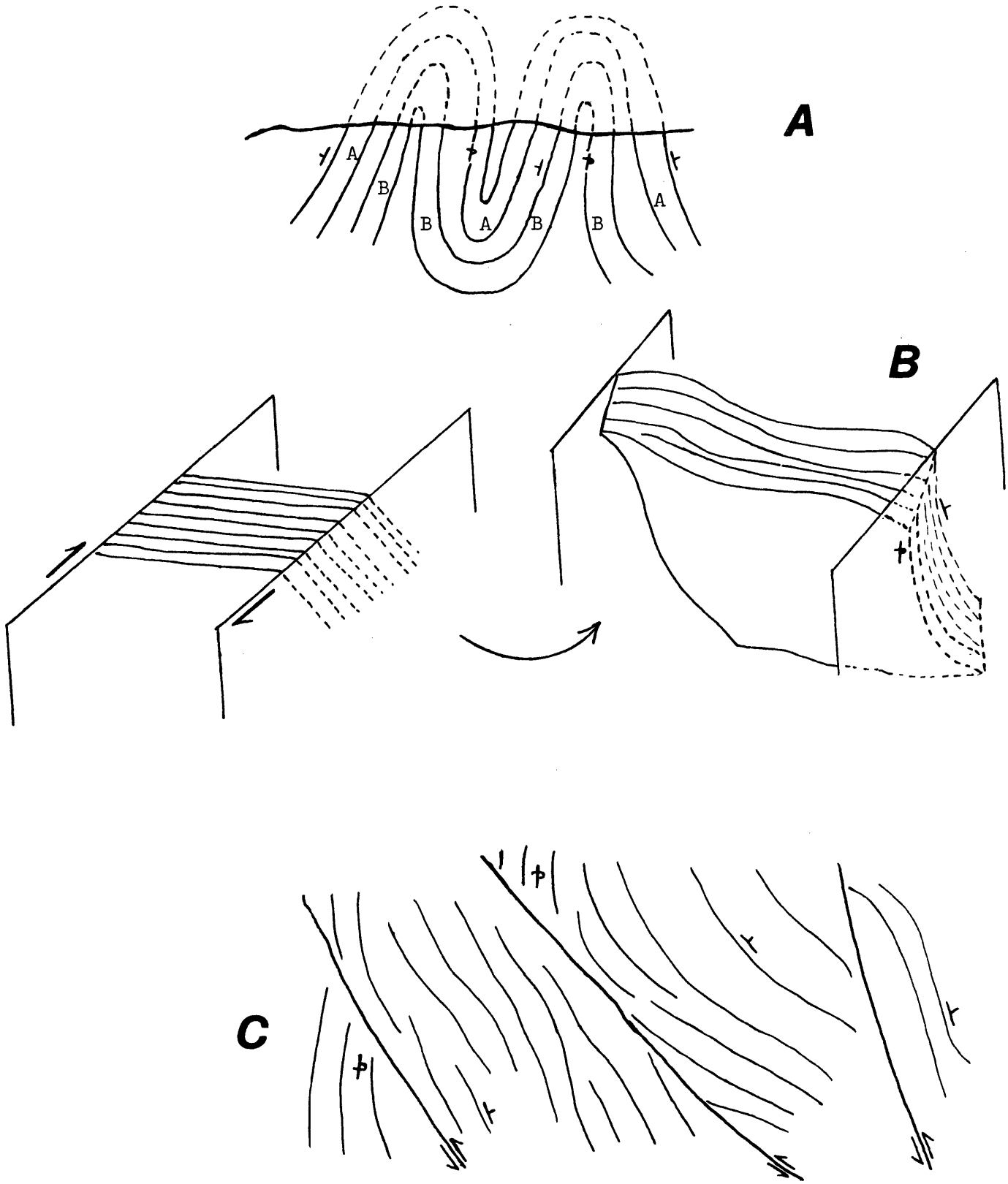


Fig. 39: Possible alternatives to explain the gentle warping of bedding and cleavage observed throughout the Coffs Harbour Block.

A: Isoclinal folding (after Lillie 1963, Fig. 5) in cross section.

B: Drag along macroscopic faults.

C: Thrust faults with only small displacements (can be either section or plan).

## POST D2 MACROSCOPIC STRUCTURES

The overall distribution of lithological units suggests that the Coffs Harbour Block could be a large complex syncline. The older units (Moombil and Brooklana Beds) are exposed on the western and southern periphery of the Block and the younger Coramba Beds generally crop out closer to the Clarence - Moreton Basin which may fill the hinge zone of the syncline. The development of the syncline is considered to be a very late stage event post-dating the mesoscopic features formed during D1 and D2. Evidence for the syncline is as follows:

(1) The headland of Red Rock appears to be the critical area in the synclinal structure. There, well bedded jaspers and cherts of the Redbank River Beds crop out. These rocks were not observed elsewhere in the Coffs Harbour Block and they separate what are probably the two limbs of the syncline occurring to the north and to the south. The two subdivisions outlined previously correlate with these two limbs.

(2) The strike of the bedding ranges from 124° to 070° and facing is to the north in sediments south of Red Rock, in contrast with strikes of 355° to 037° and facing to the west, in the north.

(3) The strike of the cleavage ranges from 137° to 078° south of Red Rock and contrasts with strikes of 000° to 049° in the north.

(4) Differences in orientation of the $B_{So}^{S_1}$ axes occur. In the southern part the fold axes vary from subhorizontal to steeply plunging and trend either to the east or to the west. This contrasts with the northern section where the fold axes are usually moderately plunging and trend either to the north or to the south.

(5) The similarity of D1 interlimb angles between the northern subdivision and the headlands of Arrawarra and Mullaway suggest these districts were possibly located along strike from each other during the time of the first deformation.

(6) The orientations of the kink bands differ between subdivisions, indicating that these kinks must have been formed prior to the formation of the syncline.

The above evidence suggests that subdivision 1 is sufficiently different in orientation to subdivision 2 to postulate the presence of a large macroscopic syncline. It is considered that this macroscopic fold

has an almost vertical axial plane striking in a WNW-ESE direction and an almost vertical fold axis. A three-dimensional sketch of the fold is presented in Figure 40.

Associated with the macroscopic syncline a series of faults dissecting the block have been inferred (Map 1). The fault surfaces are very rarely exposed and hence the dips are indeterminable but rare cases of shearing were observed. Criteria used to infer the faults include:

(1) Termination of lithologic units along their strike direction. This may be due to isoclinal folding, but no supporting evidence has been found. The three-fold subdivision of the Coffs Harbour Sequence as well as the four-fold petrogrographic subdivision of the Coramba Beds indicates, by their areal distribution, that no major repetition of lithologies by thrusting or isoclinal fold has occurred. Facing evidence indicates that the beds young consistently in one direction and the termination and displacement of particularly the units of the Coramba Beds suggests a pattern of faulting.

(2) Differences in structures occur between adjacent areas separated by the faults. Within the area bounded by two faults the strikes of bedding and cleavage appear to be consistent, but there is a difference usually of more than 5° from one fault bounded area to the next. Each fault bounded area constitutes a separate structural domain which has been subdivided on the basis of orientation patterns of mesoscopic structures. In particular, fold axes are diagnostic, plunging towards the west in one block and the plunging to the east in adjacent blocks.

(3) Discordances in metamorphic grade occur because the metamorphic zones (Map 2) appear to have been displaced across the faults. The zones, which do not coincide with stratigraphic units, are displaced so that in some places rocks from Zone II, for example, are adjacent to those from Zone IIIb.

(4) The presence of sheared and, less commonly, brecciated rocks suggest movement of some form. For example the native mercury deposit located 5 km northwest of Woolgoolga (GR 6286 2710) was found to lie in a shear zone striking almost due north, and is coincident with the position of one of the faults inferred here.

(5) The position of most of the inferred faults are coincident with linear features on aerial photographs.

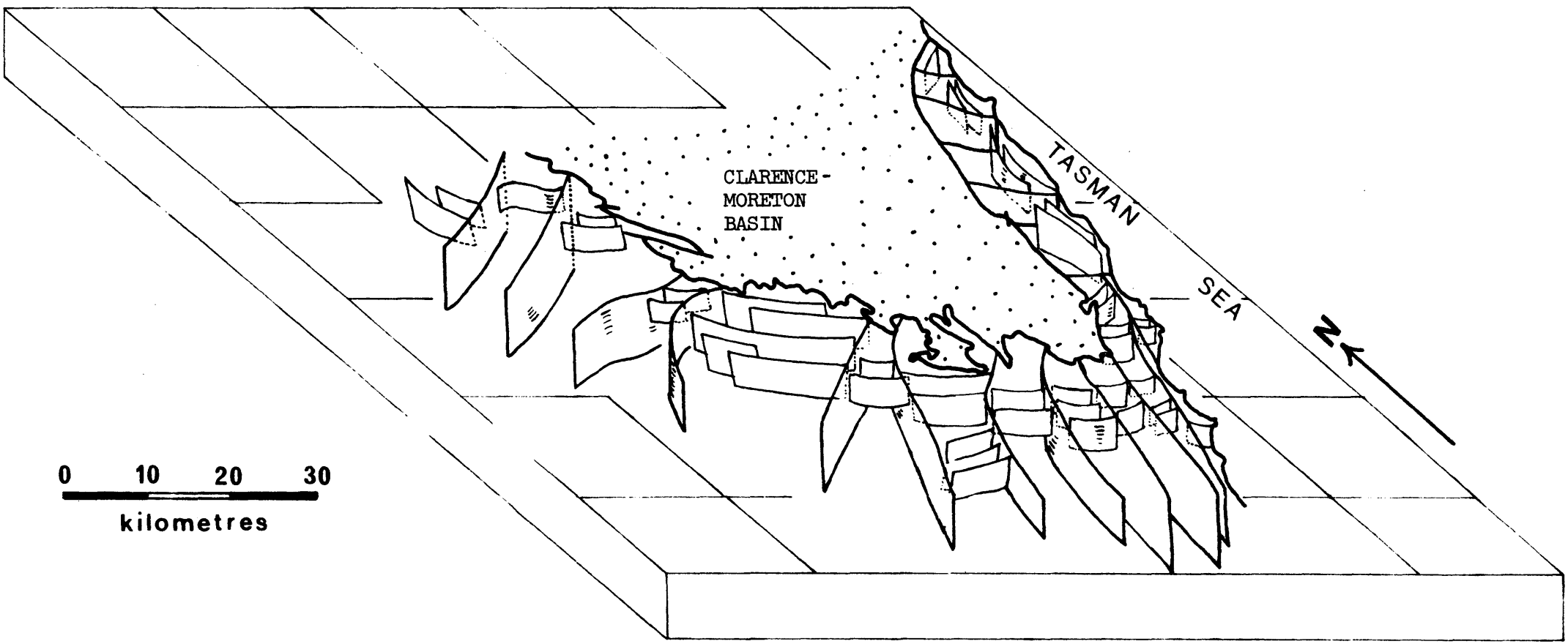


Fig. 40: Three dimensional form surfaces of the macroscopic syncline in the Coffs Harbour Block.

The faults have not been named and will be treated as a group. Because of the similar nature of all the rocks being displaced, it is considered that the main component of the movement was strike-slip. In some cases a horizontal movement of 6 km is required to realign the lithological boundaries. A slight vertical component may be present because thicknesses of the units differ across adjacent faults. It has not been possible to determine the net slip of the faults but it is possible to determine the amount of strike separations, and in most cases the movement was east block towards the south.

The nature of the syncline and associated fault pattern can be compared with a mesoscopic fold illustrated by de Sitter (1964, p.276). This fold (reproduced here as Fig. 41C) is a parallel fold in a sandstone layer from Delaware Gap, Pennsylvania. In the fold a radial fracture cleavage appears to have fractured and slightly displaced the sandstone layer. The fractures of an enlarged portion of the layer (Fig. 41B) are very similar to the inferred faults cutting the macroscopic syncline in the Coffs Harbour Block (Fig. 41A). This syncline is possibly an orocline (following the definition of Carey 1955) and its structural and tectonic implications will be discussed in Section II.

## RELATIONSHIP BETWEEN STRUCTURE AND METAMORPHISM

The cleavage in the Coffs Harbour Block grades from fracture cleavage in the north to slaty cleavage in the south. Both these types exhibit the same axial plane relationship with D1 mesoscopic folds. The slaty cleavage is defined by the preferred orientation of metamorphic phases, particularly white mica and consequently there is a very close temporal relationship between M1 metamorphism and the D1 deformation. Because of the random orientation of minerals produced by M2 it is difficult to relate M2 to any deformation and it can only be concluded to have occurred in post D1 time. Quartz veins of ages varying from pre D1 to post D2 have been identified.

## AGE OF D1, D2 AND D3

Insufficient data are available to allow precise dating of the various eposodes of deformation. However the concordant relationship of the Hillgrove type Dundurrabin Granodiorite with the regional orientation

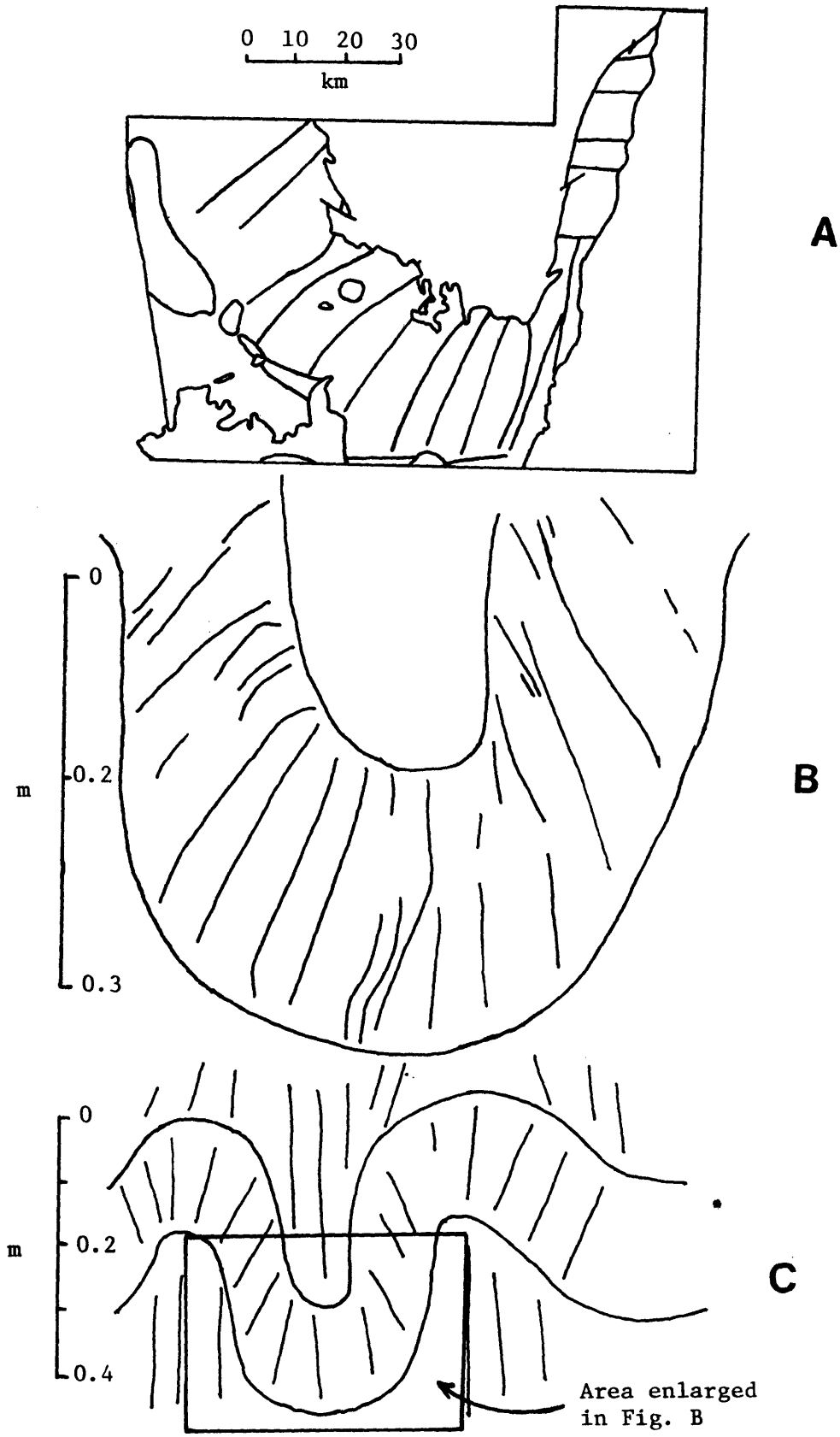


Fig. 41: Comparison of fault pattern in the Coffs Harbour Block (Fig. A) with fracture pattern in a mesoscopic fold (Figs. Band C) illustrated by de Sitter (1964, p. 276).

of the D1 cleavage suggests that D1 occurred at approximately the same time as the intrusion of the Hillgrove Suite in Early to Middle Permian time (269-252 m.y.).

The macroscopic syncline formed prior to the deposition of the Clarence - Moreton Basin, the earliest sediments of which appear to be middle-Middle Triassic in age. No evidence has been found for the continuation of the associated faults into the Mesozoic sediments and hence movement possibly ceased prior to middle Triassic time. Nevertheless the inferred position of the axial plane for the syncline occurs close to a series of east-west striking faults mapped by McElroy (1962) suggesting that movement on the axial plane might still have been taking place during the deposition of the Triassic sediments.